SOKENDAI
Graduate Institute for Advanced Studies
Department of Polar Science

Exploring spatial and temporal characteristics of current Antarctic mass change

Independent Component Analysis based on satellite geodetic data and numerical models

by

Tianyan Shi

A Dissertation submitted to
School of Multidisciplinary Sciences of the
Graduate University for Advanced Studies
In partial fulfillment of the requirement
For the degree of
Doctor of Philosophy

Supervision

Assoc. Prof. Koichiro Doi
Asst. Prof. Jun'ichi Okuno
Department of Polar Science
December 2022

Contents

List of Tables

List of Figures

Abstract

The Antarctic Ice Sheet (AIS) is the largest water and thermal energy storage on the Earth. It has been losing mass over recent decades, with potential of accelerating melting. However, the complex spatial and temporal patterns of these changes have yet to be fully understood. The mass changes in AIS results from multiple physical processes such as surface mass balance, ice dynamics, and the response of solid Earth. In order to provide new insights into the changing Antarctica, a statistical-based method named Independent Component Analysis (ICA) is applied as an analytical framework in this study.

This study qualitatively analyzes the spatial and temporal characteristics of Antarctica over the past two decades. The ICA method is used to extract independent components from complex datasets, in an attempt to separate signals from different physical sources and improve understanding of AIS mass balance. The study primarily based on satellite gravimetric observations from Gravity Recovery and Climate Experiment (GRACE) and GRACE Follow-On (GRACE-FO) missions, supplemented by satellite altimetry data from multiple missions. It also incorporates numerical models, such as the Glacial Isostatic Adjustment (GIA) and Surface Mass Balance (SMB), for examination. Firstly, six leading independent components are extracted from gravimetric data acquired during the GRACE and GRACE-FO missions. The results indicate that observed continental-scale mass changes can be effectively separated into several spatial patterns, which may be dominated by different physical processes. The overall mass changes in AIS are primarily linked to long-term mass decrease in regions such as Amundsen Sea Sector and Wikes Land in Western Antarctica, mass increase of Dronning Maud Land and Marie Byrd Land in Eastern Antarctica, as well as other periodic components. While some hidden physical processes cannot be completely isolated, significant signals like glacier melt,

snow accumulation, periodic climatic signals, and GIA effects can be determined without introducing any external information.

The altimetry data corroborates the results mentioned above. The same ICA analysis used on the GRACE/GRACE-FO data is applied to resolution-reduced altimetry data. The results reveal the remarkable influence of glaciers and snow accumulation as well, but with more complexity in high-frequency and periodic components. Comparable ICA results from both datasets demonstrate the physical significance of ICA components.

Additionally, GIA models are used to examine the separation results. A high spatial correlation is obtained by comparing the spatial distribution between models. For each AIS drainage basin, the total mass change from GRACE/GRACE-FO observations, the surface mass change derived from the SMB model, and elevation changes from altimetry are compared. Substantial differences in the time series of the basins divided them into three groups that may be dominated by different physical processes.

ICA results can be impacted by various factors, including the structure of the input data, pre-processing techniques, choice of algorithm, and number of independent components (IC). The information contained in the input data is found to impact results significantly, while the structure of the data has minimal effect. Pre-processing can enhance the separation of the object of interest when employing datasets with varying spatial resolutions. Operations such as filtering, resampling, and masking will affect the outcomes. Additionally, different ICA algorithms may be suitable for different data types. For geophysical data, particularly when the number of spatial samples is notably higher than temporal samples, sICA is recommended. The three main components of glacier change pattern, snow accumulation pattern and GIA pattern are demonstrated to be stable when adjusting the number of ICs.

Overall, ICA presents a distinctive and valuable approach to gain insights into the mass changes both at AIS-scale and further specific regional-scale. While only the linear components have been adequately interpreted and verified by this study, the remaining periodic components potentially linked to oceanic and meteorological circulation, still require further investigation.

Acknowledgements

With utmost gratitude, I express my heartfelt appreciation to all those who have supported me throughout my academic journey and helped me complete my doctoral dissertation. I wish to express my deepest gratitude to my supervisors, Prof. Doi Koichiro and Prof. Okuno Juni'chi, whose guidance and support have been invaluable in shaping my research journey. They have always been kind and gentle in their support, providing me with sufficient space to maintain my own pace of studying and work.

I also wish to express my special appreciation to Prof. Yoichi Fukuda, who accepted me as a Master's student at Kyoto University and provided me with initial guidance on my research. I still remember my first year in Japan, I always felt lost and intimidated. It was then that Prof. Fukuda handed me the key to the laboratory, which opened the door towards a place of solace and security, and opened a new chapter in my life as well.

I acknowledge Dr. J.V. Stone (https://jamesstone.sites.sheffield.ac.uk/code) for providing the ICA algorithm and code, Dr. Frederik J Simons (https://github.com/fjsimons) for the Matlab toolbox, Dr. Irie for helping me with the GIA calculation, and Prof. Niwano for providing the SMB model results.

Moreover, I would like to extend my gratitude to my colleagues and friends who have provided support and encouragement during this journey. Prof. Aoyama, Dr. Irie, Dr. Hattori, Mr. Okwa and all colleagues in NIPR, the enthusiastic atmosphere they created is an inexhaustible source of inspiration. And I would like to thank Dr. Yamamoto for always being interested in discussing my research topic.

I would like to thank my family for their boundless love, unwavering faith, and constant encouragement throughout the years. Their support has given me the courage and determination to strive towards excellence. This is an especially precious treasure for me,

as it has been extremely difficult for us to reunite and share the joys and challenges of life together since the Covid-19 pandemic. The pandemic struck at the beginning of my doctoral career, in early 2020, until today, in the Spring of 2023, my doctoral journey is coming to an end. Despite the challenges posed by the pandemic, it has been a memorable time worth commemorating. But the road of my quest has yet to come to an end. Finally, in the words of Chinese calligrapher Wang Xizhi:

"仰观宇宙之大,俯察品类之盛。"

Gazing upon the expanse of the universe, and surveying the richness of all things.

We stand in the shadow of giants who have preceded us, with each step, we inch closer to the stars.

施 天焰

Tianyan Shi

Tokyo, Japan

March, 2023

Chapter 1

Introduction

The AIS mass migrates to the ocean through a network of glaciers that basically determined by the topography. Fluctuations in AIS mass result from differences between net snow accumulation at the surface, runoff, and ice flux to the ocean. The AIS had maintained a dynamic equilibrium until recent decades. A series of satellite missions have been launched since the late 20th century, providing favorable conditions for the continuous monitoring of Antarctic mass changes. The accumulation of different types of data not only facilitates the estimation of the AIS mass balance but also enables further analysis of the spatiotemporal characteristics of Antarctic variability.

Many studies have reported the accelerated melting of the AIS in recent years (e.g., Shepherd et al., 2012; Velicogna and Wahr, 2013; The IMBIE team, 2018). The accurate calculation of the AIS mass/volume changes is important not only for sea-level changes (van den Broeke et al., 2009) but also for many aspects of the Earth's environmental system. For example, the melting of the ice shelf affects the thermohaline circulation, sea ice coverage affects the albedo (Massom and Stammerjohn, 2010). With the current critical situation in Antarctica, monitoring of the AIS changes has become particularly important.

AIS is a complex system. The interactions among its sub-components, such as atmosphere, snow/ice, and solid Earth, have not been well understood. The heterogeneous spatiotemporal variability in Antarctica changes can be attributed to the varying sensitivity of different physical processes.

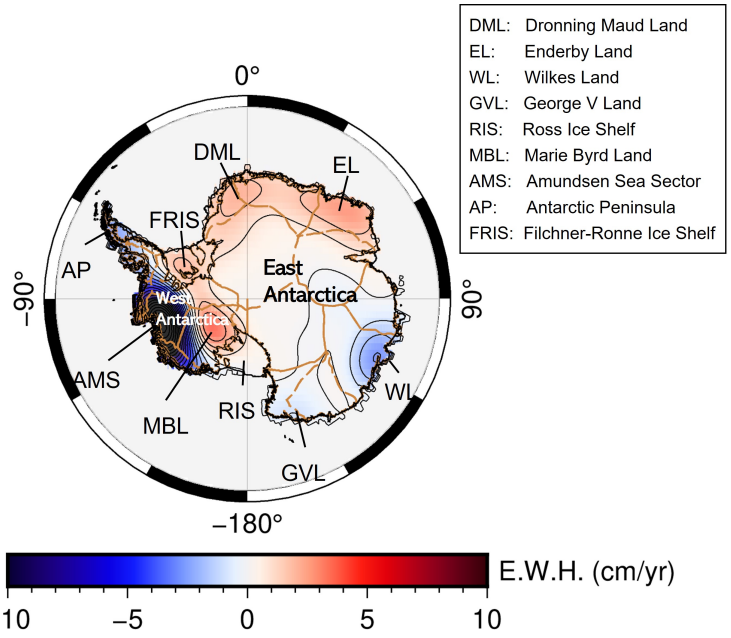

Figure 1.1: Trend of Antarctic mass change between April 2002 and June 2020 derived from GRACE/GRACE-FO.

As shown in Fig. 1.1, the trend of mass changes in Antarctica has been determined through satellite gravimetric observations using a simple linear regression model (considering only the linear term). The mass changes are expressed in equivalent water height (E.W.H.). It can be observed that the mass changes are primarily concentrated in several areas:

1. Significant mass loss in the Amundsen Sea Sector (AMS), West Antarctica (WA), and Bellingshausen Sea Sector, Antarctic Peninsula (AP);

2. Significant mass gain across Dronning Maud Land (DML) and Enderby Land (EL), East Antarctica (EA);

3. Mass loss across Totten Glacier in Wilkes Land (WL) and Ninnis Glacier in George V Land (GVL), EA;

4. Mass gain across the Ross Ice Shelf (RIS), Filchner-Ronne Ice Shelf (FRIS) and a portion of Marie Byrd Land (MBL), WA.

It can be observed that the mass variation is more concentrated in the coastal zone of Antarctica than in the vast interior area. Moreover, significant discrepancies in trends are observed between EA and WA. For instance, a strong long-term mass reduction trend is observed in the AMS, which contributes to more than 60% of the total mass loss (Rignot et al., 2019). This trend is three times larger than that from EA, where a remarkable trend of decreasing is not observed, except for some glacial areas (e.g., WL).

Regarding the specific situation of each sub-basin, it varies depending on the dominant physical mechanism. For example, the deceleration of glaciers of the RIF could be determined by submarine topography. In some coastal regions like AP, dramatic seasonal fluctuations can be observed, which may be due to frequent sea-ice-atmosphere interactions.

Beneath the thick layer of ice sheet, differences in the rheological properties of EA and WA are another important factor that contributes to the spatial heterogeneity of Antarctica's long-term trend. In particular, the response of the solid Earth to the ice-ocean loading following the Last Glacial Maximum (LGM), known as glacial isostatic adjustment (GIA), has a direct impact on satellite measurements. Therefore, in addition to estimating mass loss in Antarctica, it is equally important to study the spatial and temporal characteristics of the Antarctic changes to better understand its response to global climate change.

1.1 Motivation and Research Aim

1. Regarding the recent changes in AIS mass, extensive investigation has been facilitated by recent developments in satellite observations. As mentioned above, previous studies focused on the mass balance of AIS and have revealed its accelerating melting. However, due to the complexity and heterogeneity of the AIS changes both temporally and spatially, despite these efforts, there still exist considerable gaps in our understanding of specific temporal and spatial characteristics of AIS variability that require further exploration. In particular, the characteristics of the various physical components of AIS lack investigation from the perspective of geodetic observation.

2. Satellite geodetic observations usually contain the superposition of multiple physical signals. Physical models such as GIA and meteorological models are commonly used to determine the corresponding sub-components. However, it will inevitably introduce human bias in estimating AIS mass changes and will further interfere with the understanding of the physical mechanisms of the AIS system. For instance, GIA plays a vital role in understanding the interaction between the solid Earth and ice sheet changes. However, the harsh conditions in Antarctica make it impossible to rely on Global Navigation Satellite System (GNSS) observations to constrain GIA models on a continental scale, leading to significant uncertainty in estimating AIS mass balance. Therefore, it is worth reconsidering fully utilizing the accumulated multi-satellite data to explore physical processes further from observational data.

3. For each drainage basin in AIS, there is significant variation in the dominant physical processes. For instance, coastal regions tend to experience higher snowfall compared to inland areas; areas with intense melting are typically dominated by glacier discharge. Unlike the AIS as a whole, these physical processes are more distinguishable and readily apparent in each basin. Additionally, different observations have varying sensitivities in detecting specific physical processes (refer to Sec. 2.1). Therefore, the regional study could be a crucial entry point for understanding the spatial characteristics of AIS.

Therefore, this study aims to focus on two topics. Firstly, exploring the spatiotemporal characteristics of Antarctic mass changes, with a particular focus on variability within various physical processes, such as snowfall and glaciers. Secondly, investigating the underlying physical mechanisms behind these changes by tracing variations in physical sources, and attempting to improve the modeling using satellite data.

By analyzing the changing characteristics of each component, it is possible to deepen the understanding of the spatiotemporal characteristics of the Antarctic ice sheet (AIS) changes. Moreover, investigating the interaction within sub-components and identifying common drivers could further facilitate the possibility of revealing the response of the

AIS to oceanic/atmospheric circulation and global climate changes.

To achieve these objectives, combined satellite observation data will be used. Making full use of the statistical information of datasets of the AIS changes could be a worthwhile approach. A statistical-based method named independent component analysis (ICA) is applied as an analytical framework in this work to provide a new perspective for understanding the changing Antarctica.

1.2 Structure of Dissertation

Chapter 1 includes basic information about Antarctica, the purpose of the study, and the structure of this dissertation.

Chapter 2 provides a detailed introduction of main compositions of the Antarctic mass changes and possible physical processes. The second part describes some common satellite geodetic methods that can be used for Antarctic observations, as well as their advantages and limitations, and the research progress achieved so far using these methods.

Chapter 3 presents the main method used in this study, namely independent component analysis (ICA), and provides a brief review of the application of ICA in extracting geophysical signal.

Chapter 4 presents the results of ICA, which is mainly derived from satellite gravity data supplemented by satellite altimetry data. Additionally, this chapter discusses suitable methods for merging two different datasets that vary widely in spatial resolution and spatial coverage.

Chapter 5 interprets the results of ICA in combination with numerical models, mainly introducing the GIA models and Regional Climate Model (RCM). It also analyzes subregions of Antarctica and presents changes characteristic in each drainage basin.

Chapter 6 discusses better ways to apply ICA to achieve more reasonable results and avoid treating ICA as a black box. This chapter covers factors that can affect ICA results, such as the period of input data, filters, and suitable scenarios of different algorithms. The chapter also describes a series of pre-processing steps and evaluates the stability in extracting the required information.

Chapter 7, the conclusion and outlook. This chapter reviews the overall research concept and content of this dissertation. Finally, the weaknesses of current work and future research directions are discussed.

Chapter 2

Background

2.1 Physical Processes in Antarctica

The physical processes that occur in Antarctica can be roughly categorized into three sources: the atmosphere, the ice-sheet surface, and the solid Earth. This section introduces the primary physical processes in each layer from the perspective of satellite observations. The mass input and output processes across the AIS system can assist in interpreting the physical processes.

2.1.1 Surface Mass Balance

Surface mass balance (SMB) analysis can be employed to estimate the atmospheric variations across the AIS surface, with a particular focus on snowfall, rainfall, surface sublimation, drifting snow sublimation and other sources (Van Den Broeke et al., 2004). It can be expressed as:

$$S = P + R - U_s - U_{ds} - E_{ds} - M, \tag{2.1}$$

where S is SMB, P is precipitation, R is rainfall, U_s and U_{ds} are surface sublimation and drifting snow sublimation, E_{ds} is erosion of snow and M is melting runoff.

The input of the AIS system is mainly contributed by precipitation, especially from snowfall. In areas where SMB is negative ($S < 0$), it is the ablation zone and where it is positive ($S > 0$), it is accumulation zone. In the accumulation zone, snow will accumulate year by year and gradually be compressed into firn/ice under its own weight, with density

increasing with depth. This process varies largely from area to area depending on the local climate and the precipitation rate.

SMB generates about 2500 $Gt/year$ mass input in Antarctica (Agosta et al., 2019). It reflects directly on the gravitational field, and the accumulated mass will disturb the gravitational potential field above the surface correspondingly. The SMB also causes fluctuations in the volume of the AIS. In the accumulation zone, the surface elevation is in a continuous trend of rising. At the same time, firn compaction causes decreasing of surface elevation, the rate can be empirically estimated according to annually-averaged temperature, precipitation, and wind speeds. Generally, firn compaction affects only the surface elevation changes and has negligible impact on gravity field.

However, the conversion from elevation change to mass change requires an external Firn Densification Model (FDM) or a proper density model which is highly limited by the sparse observation networks of surface SMB. It is difficult to accurately estimate the snow-firn-ice density over the whole Antarctic continent, which makes the conversion process contain a huge error (Zwally et al., 2011).

As a meteorologic dominant component, there are seasonal variations at the annual scale, such as the strongest melting occurring during the austral summer (Liston et al., 1999). Glacier melting may be ocean-driven at medium- to long-term scales (Pritchard et al., 2012; Hirano et al., 2020), whereas it may be determined by topography and ice shelf stability at the long-term scale.

In summary, SMB causes changes in both gravity field and elevation. There are significant seasonal variations in SMB and a distinctive coast-inland decrease in the precipitation gradient owing to the moisture air masses decreasing as they migrate onto the Antarctic Plateau. Firn compaction is the main uncertainty source for SMB observation.

2.1.2 Ice Dynamics

As mentioned in Sec.2.1.1, mass (mostly snow) accumulates in the accumulation zone and transformed into glacier ice over a long period of time. The mass loss through erosion of snow E_{ds} and melting runoff M is less than 100 Gt/yr according to some regional climate models (RCM), like RACMO and MAR (van Wessem et al., 2018; Agosta et al.,

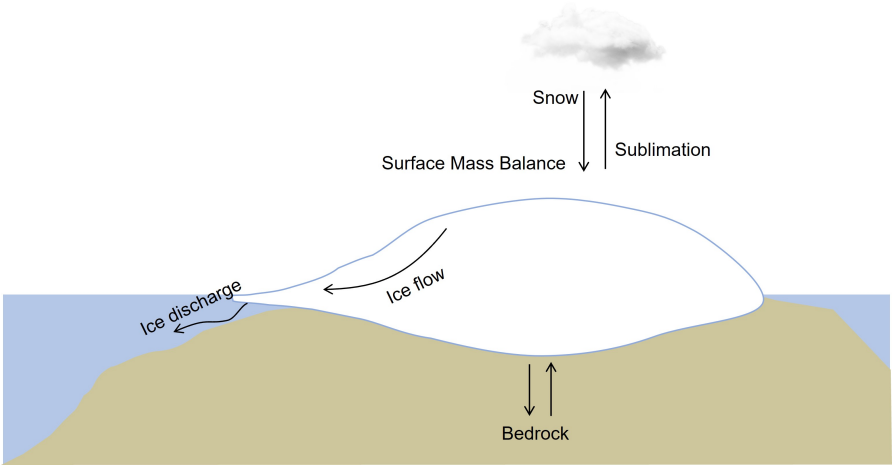

Figure 2.1: Mass balance and basic physical processes in the Antarctic.

2019), which means the regressing of AIS is attributed mainly to the ice dynamics process through melting glaciers.

Ice dynamics describes the continuous motion of glaciers caused by gravity from upstream to downstream, where they melt into the ocean. This process may be accompanied by glacier thinning, resulting in a simultaneous decrease in elevation and geopotential.

Ice dynamics is another long-term process that is determined mainly by temperature and the pressure on bases. Thus, it can be considered as a relatively constant trend in mass and elevation change. Ice velocity varies greatly from basin to basin, depending on topography and other conditions. Quantifying it's contribution to AIS changes requires measurements of thickness and ice velocity of glaciers, which can be obtained using altimeters and interferometric synthetic aperture radar (InSAR). However, unlike the SMB, some ice discharge processes are not directly reflected in surface elevation since the melting occurs on the bottom of the ice shelf. Consequently, this portion of mass discharge through the bottom melting at the grounding line uncertainty still remains.

2.1.3 Solid Earth

The loading on the Earth's surface causes deformation of the solid Earth. GIA, the on-going response of the solid Earth due to changes in the ice/ocean loading following the

Last Glacial Maximum (LGM), is also an essential contributor to current AIS changes. Strictly, the GIA effect is not a part of AIS, but as the basis of AIS, a proper understanding of GIA is the key to understanding interactions among each component in Antarctica.

The ice/ocean loading is directly supported by the lithosphere and upper-most mantle. The effect of GIA under the same loading history depends on the material properties of these two spheres; i.e. the rheology of the solid Earth. Besides that, there is large uncertainty in loading history itself as well.

In addition to the direct deformation of bedrock, the accompanying redistribution of near-surface solid Earth also affects the geopotential. It can be found that the factors that determine GIA can all be considered as constant on the time scale of current satellite observations (a few decades). Therefore, GIA can be regarded as another linear trend in mass and elevation changes and is far more stable and long lasting compared to ice dynamics described in Sec.2.1.2.

However, sparse in-situ observation networks across Antarctica have led to the inability to effectively constrain the GIA effect, with this effect possessing the dominant uncertainty in AIS mass balance estimations. Numerous approaches have been proposed to constrain the GIA effect, such as joint analyses of GRACE/GRACE-FO data and either global positioning system (GPS) (Wang et al., 2013; Hattori et al., 2021) or Satellite altimeter data (Wahr et al., 2000; Riva et al., 2009).

The detailed modeling is beyond the scope of this work, but instead, some current GIA models will be introduced in Chapter 5 as references for ICA analysis.

2.2 Geodetic Observation for Antarctica Mass Changes

The AIS changing signals described above can be obtained from different geodetic methods, mainly through elevation and geopotential changes (Fig. 2.2).

2.2.1 Gravity

Satellite gravity method, in particular, Gravity Recovery and Climate Experiment Mission (GRACE) launched in 2002 and it's successor GRACE-Follow on (GRACE-FO)

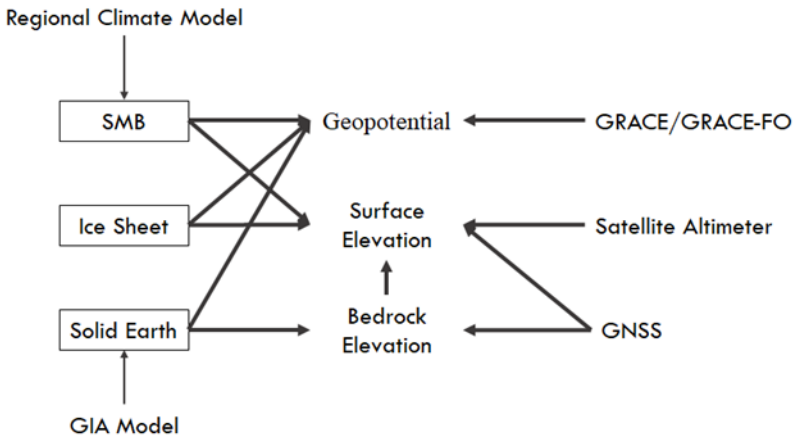

Figure 2.2: The effect of physical processes in the Antarctic and geodetic observations.

launched in 2018 have provided the conditions for direct observation of mass changes over the Antarctic continental scale.

The GRACE/GRACE-FO consists of two separate identical satellites that run in tandem on the same orbit about 500 km above the ground. The K-band ranging system (KBR) is equipped on the satellites to enable precise inter-satellite ranging. In addition, the satellites are equipped with GPS receivers to observe precise satellite position and accelerometers to eliminate the effects of non-conservative forces before gravity field modeling. The time-varying Earth's gravity field model can be obtained by continuously measuring the change of the distance between two satellites. GRACE/GRACE-FO orbits can completely cover Antarctica with a native spatial resolution of about 300 km and a temporal resolution of about one month.

GRACE/GRACE-FO observe the superposition of gravity changes caused by different physical processes along the radius, including changes from atmospheric, oceanic and the solid Earth. It is difficult to extract specific signals from the total mass changes. In order to use GRACE/GRACE-FO observation data to study specific physical processes, some post-processing methods for time series analysis are necessary to separate different physical signals from each other.

In recent years, AIS mass changes have been extensively studied using the GRACE/GRACE-FO data. For example, Velicogna and Wahr (2006) estimated the melting rate of Antarc-

Table 2.1: Geodetic Observations for Antarctica

Observation		Type	Physical Processes	Coverage
GRACE/GRACE-FO		Gravity Field	GIA, SMB, Ice	90°S-N
Altimeter	Seasat	Surface elevation	GIA, SMB, Firn, Ice	72°N-S
	ERS-1/ERS-2			81.5°N-S
	ICESat			86°N-S
	CryoSat			88°N-S
GNSS		Bedrock elevation	GIA	Regional

tic ice sheets to be $-152 \pm 80\ Gt/yr$ using CSR RL01 data from April 2002 to August 2005, by subtracting the GIA effects with IJ05 model (Ivins and James, 2005), that most of the ice sheet melting occurred in West Antarctica. Similarly, Chen (2006) studied the AIS mass changes using CSR RL01 data from April 2002 to November 2005. A $500-km$ Gaussian filter was applied to suppress the model noise, and the same GIA model (IJ05) was used to deduct the GIA effects. The results showed that the melting of West AIS is mainly concentrated near the coastline, and the mass increase of East Antarctica is mainly concentrated in the Enderby Land area.

King et al. (2012) estimated the melting rate of the AIS to be $-69 \pm 18\ Gt/yr$, and its contribution to sea-level rise to be $0.19 \pm 0.05\ mm/yr$ using CSR RL04 data from August 2002 to December 2010 and deducted the GIA effects from W12a model.

Luthcke et al. (2013/ed) determined the ice mass evolution of the AIS, Greenland ice sheets (GIS) and Gulf of Alaska (GoA) from a new GRACE solution of Mass concentration (mascons). For the time period December 2003 to December 2010, the total melting rate was estimated to be $-380 \pm 31\ Gt/yr$ with an acceleration of $-41 \pm 27\ Gt/yr^2$. Its contribution to sea-level rise to be $1.05 \pm 0.09\ mm/yr$ with acceleration of $0.11 \pm 0.08\ mm/yr^2$.

A note is that the Earth's internal material redistribution accompany with GIA has a direct impact on satellite gravity measurements (Wahr et al., 2000). All of the above studies indicated that GIA is the dominant uncertainty in the AIS mass estimation.

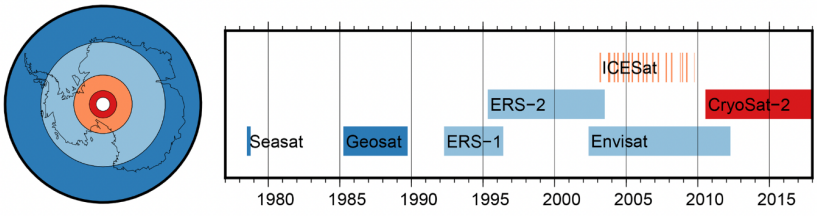

Figure 2.3: Data coverage of satellite altimeter missions. ((Schröder et al., 2019))

GRACE/GRACE-FO missions provide direct observations of AIS masses including the basal melting of glaciers while not being affected by Firn compaction, but it is also more sensitive to material redistribution caused by GIA. Some regionally important processes, such as drifting snow sublimation, might have a negligible impact on the SMB at the GRACE/GRACE-FO spatial resolution (van Wessem et al., 2018).

2.2.2 Elevation

The earliest monitoring of the Antarctic based on satellite altimetry technology can be traced back to the late 1970s, when an Earth-orbiting satellite, Seasat was launched which was designed for remote sensing of the Earth's ocean. After a gap of about seven years, Geosat with a similar 108°inclination orbit was launched in 1985. However, the spatial coverage of Seasat and Geosat was limited to 72°N-S, which could only cover the northern tip of the Antarctic Peninsula and the coastal regions of the EA (Fig. 2.3). Since 1992, European Remote-Sensing Satellite-1 (ERS)-1, ERS-2, and Environmental Satellite (Envisat) have been launched that widen spatial coverage to cover 81.5°N-S latitude, and largely enhanced the capability to monitor polar regions. But their spatial resolution is relatively coarse, especially when performing in ice mode for the purpose of capturing the radar return from rough topographic surfaces.

Spatial coverage continues to expand with Ice, Cloud, and land Elevation Satellite (ICESat) (86°N-S) and CryoSat-2 (88°N-S), leading to nearly complete coverage of the AIS in recent epochs and providing higher spatial resolution and intensive repeat observations. Altimeter observations include the signals from SMB, ice dynamics and GIA. While considering the observation coverage history and the rate of ice dynamics up to (0.5 m/yr),

the bedrock deformation caused by GIA (few cm/yr) is not as significant as that in GRACE/GRACE-FO.

Wouters et al. (2015) combined ICESat, Envisat, and CryoSat-2 altimeter data to estimate the mass balance of the Antarctic Peninsula from 2003-2009 and 2010-2014, and compared the glacier mass changes between the two time periods, finding the accelerated melting glaciers on the Antarctic Peninsula.

The mass balance of all Antarctic basins was estimated by Shepherd et al. (2019). The elevation change of AIS is measured based on multiple satellite altimeter data (including ERS-1, ERS-2, Envisat, and CryoSat-2) and is converted to mass balance using surface density model.

Furthermore, there are also geodetic observations such as Global Navigation Satellite System (GNSS), InSAR as mentioned above and other remote sensing methods. GNSS can provide continuous vertical displacement records with extremely high precision of bedrock and can effectively constrain GIA process. GRACE/GRACE-FO and altimeter datasets are mainly used for analysis. The utilization of GNSS and remote sensing data is not in the scope of this work.

In summary, The altimetry method can directly measure the surface elevation change that simultaneously derived from SMB, firn compaction and bedrock deformation of GIA. The volume changes can be converted to mass changes by a specific density. The density estimating for surface density contains considerable uncertainty, especially for firn compaction.

The satellite gravimetric method can obtain AIS mass changes directly from gravity field data. However, the wildly applied satellite missions GRACE/GRACE-FO capture the vertical integration of all components. Its products lack vertical resolution and have low spatial resolution relative to the altimeter and GNSS data.

Chapter 3

Statistics Based Signal Separation Methods

3.1 Method

3.1.1 Principal Component Analysis (PCA)

Due to the sampling of time-varying geophysical field, a huge amount of data will be produced. The purpose of Principal Component Analysis (PCA) method is to reduce the dimensionality of the data and determine the most important temporal and spatial characteristics of gravity changes. PCA is widely used to extract principal modes of data while also suppressing weak signals and noises. The modes obtained by PCA are uncorrelated rather than independent, which means the principal components are a series of mixtures of physical processes. PCA is usually used as a pretreatment for ICA.

Here take GRACE/GRACE-FO gravity field as an example, GRACE observations build on a data matrix $\boldsymbol{X}$ with $\boldsymbol{n}$ grids and $\boldsymbol{p}$ epochs, as

$$\boldsymbol{X} = (\boldsymbol{x_1}, \boldsymbol{x_2}, \boldsymbol{x_3}, \cdots, \boldsymbol{x_p})^{\boldsymbol{T}} = \begin{pmatrix} \boldsymbol{x_{1,1}} & \boldsymbol{x_{1,2}} & \cdots & \boldsymbol{x_{1,p}} \\ \boldsymbol{x_{2,1}} & \boldsymbol{x_{2,2}} & \cdots & \boldsymbol{x_{2,p}} \\ \vdots & \vdots & \ddots & \vdots \\ \boldsymbol{x_{n,1}} & \boldsymbol{x_{n,2}} & \cdots & \boldsymbol{x_{n,p}} \end{pmatrix} \tag{3.1}$$

Then the covariance matrix $\boldsymbol{C}$ of the data can be calculated, and the covariance matrix

contains the variance and covariance information for each grid point and epoch.

$$\boldsymbol{C} = \frac{\mathbf{1}}{\boldsymbol{p}}\boldsymbol{X}\boldsymbol{X}^{\boldsymbol{T}} = \frac{\mathbf{1}}{\boldsymbol{p}}\begin{pmatrix} \sum_{i=1}^{p} \boldsymbol{x}_{1,i}^{2} & \sum_{i=1}^{p} \boldsymbol{x}_{1,i}\boldsymbol{x}_{2,i} & \cdots & \sum_{i=1}^{p} \boldsymbol{x}_{1,i}\boldsymbol{x}_{n,i} \\ \sum_{i=1}^{p} \boldsymbol{x}_{2,i}\boldsymbol{x}_{1,i} & \sum_{i=1}^{p} \boldsymbol{x}_{2,i}^{2} & \cdots & \sum_{i=1}^{p} \boldsymbol{x}_{2,i}\boldsymbol{x}_{n,i} \\ \vdots & \vdots & \ddots & \vdots \\ \sum_{i=1}^{p} \boldsymbol{x}_{n,i}\boldsymbol{x}_{1,i} & \sum_{i=1}^{p} \boldsymbol{x}_{n,i}\boldsymbol{x}_{2,i} & \cdots & \sum_{i=1}^{p} \boldsymbol{x}_{n,i}^{2} \end{pmatrix} \tag{3.2}$$

The total variance can be obtained by summing the independent variances in the covariance matrix, the total variance is equal to the trace of the covariance matrix:

$$\boldsymbol{\Delta^2} = \frac{\mathbf{1}}{\boldsymbol{p}} \sum_{j=1}^{n} \left(\sum_{i=1}^{p} \boldsymbol{x}_{j,i}^{2} \right) = \mathbf{trace\,(C)} \tag{3.3}$$

The purpose of PCA is to find a set of vectors $\boldsymbol{e} = (\boldsymbol{e_1}, \boldsymbol{e_2}, \boldsymbol{e_3}, \cdots, \boldsymbol{e_p})^{\boldsymbol{T}}$ in the original data X and maximizes the projection variance of $\boldsymbol{X}$ on eigenvector $\boldsymbol{e}$. These $\boldsymbol{e}$ are known as Empirical Orthogonal Functions (EOF). The variance of the projection can be expressed as:

$$\boldsymbol{Var\,(Xe)} = \boldsymbol{e^T C e} \tag{3.4}$$

The eigenvalue decomposition of the covariance matrix can solve the problem of projection maximization:

$$\boldsymbol{Ce} = \boldsymbol{\lambda_i^2 e} \tag{3.5}$$

$$\boldsymbol{C} = \boldsymbol{EAE^T} \tag{3.6}$$

Where $\boldsymbol{\lambda}$ is an eigenvalue of matrix $\boldsymbol{C}$, $\boldsymbol{A}$ is a diagonal matrix contains n eigenvalues $\boldsymbol{\lambda_i}$, the column of the orthogonal matrix $\boldsymbol{E}$ contains the corresponding eigenvector $\boldsymbol{e_i}$. Since the sum of all eigenvalues is equal to the trace of the covariance matrix $\boldsymbol{C}$ and the total variance is equal to the trace of the covariance matrix, the sum of the eigenvalues is also equal to the total variance:

$$\sum_{j=1}^{n} \boldsymbol{\lambda_j} = \boldsymbol{\Delta^2} \tag{3.7}$$

Arrange the eigenvalues and corresponding eigenvectors according to the eigenvalues in descending order. Make each eigenvalue on the diagonal of matrix $\boldsymbol{A}$ to be $\boldsymbol{\lambda_1 \geq \lambda_2 \geq \cdots \geq \lambda_n}$. The amount of information "interpreted" by each eigenvector can be expressed as:

$$\boldsymbol{n_j = 100\% \times \frac{\lambda_j}{\Delta^2}} \tag{3.8}$$

PCA uses the eigenvectors of matrix C as the basis vectors to express the original observation data $\boldsymbol{X}$. Moreover, the eigenvectors need to be normalized to make $\boldsymbol{e_j^T e_j = 1}$. The first mode of the empirical orthogonal function contains the main features of the spatial domain.

$$\boldsymbol{x_i = d_{1,i}e_1 + d_{2,i}e_2 + \cdots + d_{n,i}e_n = \sum_{j=1}^{n} d_{j,i}e_j = Ed_i} \tag{3.9}$$

Since $\boldsymbol{E^T E = I}$, eq.3.9 can also be written as $\boldsymbol{d_i = (E^T E)^{-1} E^T x_i}$.
In addition, the ordinary PCA method can be extended by rotating EOF (Richman, 1986).

3.1.2 Independent Component Analysis

ICA is a method for decomposing mixtures of source signals into statistically independent components (ICs), which can utilize the statistical characteristics of observation data like GRACE to explore the potential signals without any prior information. ICA uses higher-order statistics information (usually forth-order moment (kurtosis) or entropy) to find independent components. While the observations of GRACE exhibit non-Gaussian properties, the high-order statistical information derived from them is not accounted for by PCA (Forootan and Kusche, 2012).
Based on Bell and Sejnowski (1995), ICA can contrive to find ICs even if the underlying sources are not statistically independent. Therefore, ICA can find the independent signals which are not the underlying sources. The data matrix $\boldsymbol{X}$ with the same building as 3.1, can be considered as a linear combination of a series of independent signals. This process can be expressed as:

$$\boldsymbol{X = AS,} \tag{3.10}$$

where $\boldsymbol{A}$ is an unknown mixing matrix. To recover the original signals $\boldsymbol{S}$, let unmixing matrix $\boldsymbol{W} = \boldsymbol{A^{-1}}$ thus,

$$\boldsymbol{S = WX.} \tag{3.11}$$

The purpose of any ICA algorithm is to find the unmixing matrix $\boldsymbol{W}$. Here, maximum likelihood estimation is used to explain the algorithm. In the original paper of Bell and Sejnowski (ibid.), a complicated idea called the infomax principle was introduced to explain the algorithm. But that is no longer necessary because the infomax principle is considered equivalent to maximum likelihood estimation (Cardoso, 1997).

Suppose that the probability density distribution for each source signal $\boldsymbol{s_i}$ is $\boldsymbol{p_i}$ and the joint distribution of source $\boldsymbol{S}$ is:

$$\boldsymbol{S = \prod_{i=1}^{n} p_s(s_i).} \tag{3.12}$$

The joint distribution is modeled as the marginal and the source signals are assumed to be independent according to Eq.3.11, we can find the probability density of the observation variable $\boldsymbol{X}$ as:

$$\boldsymbol{p(X) = \prod_{i=1}^{n} p_s(w_i^T) \cdot |W|\,.} \tag{3.13}$$

To specify the density of $\boldsymbol{s_i}$, we need to specify a monotonically increasing Cumulative Distribution Function (CDF) for it. A CDF has to be non-Gaussian, as ICA doesn't work on Gaussian data. A reasonable function that can slowly increase from 0 to 1, such as the sigmoid function $\boldsymbol{g(s) = 1/(1 + e^{-s})}$ will be chosen. There is $\boldsymbol{p(s) = g'(s)}$. $\boldsymbol{W}$ is the parameter matrix of the model. Given a training set $\boldsymbol{\{x_i | i = 1, ..., m\}}$, of which log-likelihood is:

$$\boldsymbol{\ell(W) = \sum_{i=1}^{m}(\sum_{j=1}^{n} \log g'(w_j^T x_i) + \log|W|).} \tag{3.14}$$

We can easily derive a stochastic gradient descent learning rule to maximize the likelihood with $\boldsymbol{W}$ based on the fact $\boldsymbol{\bigtriangledown_W |W| = |W|(W^{-1})^T}$. There are two extension forms for ICA called spatial ICA (sICA), temporal ICA (tICA), and their combination, spatio-temporal ICA (stICA). ICA can be considered as a rotation extension of PCA or singular

value decomposition (SVD) (Comon, 1994). Usually, $\boldsymbol{X}$ can be decomposed by SVD to reduce its rank:

$$\boldsymbol{X \approx UDV^t.} \tag{3.15}$$

Where $\boldsymbol{U}$ is a $\boldsymbol{n \times k}$ matrix that contains all eigenimages, $\boldsymbol{V}$ is a $\boldsymbol{p \times k}$ matrix that contains all eigensequences, $\boldsymbol{D}$ is a $\boldsymbol{k \times k}$ diagonal matrix of singular values. Eq.3.15 can be written as follows:

$$\boldsymbol{X \approx UDV^t = \tilde{U}\tilde{V}^t = UD^{1/2}D^{1/2}V^t,} \tag{3.16}$$

where $\boldsymbol{\tilde{U} = UD^{1/2}}$ and $\boldsymbol{\tilde{V} = VD^{1/2}}$.

Considering that $\boldsymbol{S = (s_1, s_2, \ldots, s_k)}$ contains the spatial independent vectors, $\boldsymbol{k}$ is the number of eigenvectors. $\boldsymbol{T = (t_1, t_2, \ldots, t_k)}$ contains the temporal independent vectors. The linear combinations of spatial independent signals S are in the column vectors of $\widetilde{\boldsymbol{U}}$, analogously, temporal independent signals T are in $\widetilde{\boldsymbol{V}}$. Thus, $\widetilde{\boldsymbol{X}}$ can be decomposed as:

$$\boldsymbol{\widetilde{X} = S\Lambda T^t.} \tag{3.17}$$

where $\boldsymbol{\Lambda}$ is a diagonal matrix of scaling parameters.

Spatial ICA (sICA) can find a series of spatial independent components and corresponding time series. sICA assumes that $\widetilde{\boldsymbol{U}}$ can be decomposed as $\widetilde{\boldsymbol{U}} = \boldsymbol{SA_S}$, $\boldsymbol{A_s}$ is a $\boldsymbol{k \times k}$ mixing matrix, $\boldsymbol{S}$ is a statistical independent matrix of spatial vectors. Thus, the scaled original signal $\boldsymbol{y_{s_i} = \widetilde{U}W_s}$ can be recovered by the unmixing matrix $\boldsymbol{W_s}$, where $\boldsymbol{W_s = A_s^{-1}}$.

Temporal ICA (tICA) can find a series of temporally independent components and corresponding spatial vectors. tICA assumes that $\widetilde{\boldsymbol{V}} = \boldsymbol{TA_T}$, $\boldsymbol{A_T}$ is a $\boldsymbol{k \times k}$ mixing matrix, $\boldsymbol{T}$ is a statistical independent matrix of time series. Thus, the scaled original signal $\boldsymbol{y_{s_i} = \widetilde{U}W_T}$, can be recovered by the unmixing matrix $\boldsymbol{W_T}$, where $\boldsymbol{W_T = A_T^{-1}}$.

Spatiotemporal (stICA) can simultaneously maximize the degree of independence of components over time and space. stICA assumes that $\widetilde{\boldsymbol{X}}$ can be decomposed into

$\widetilde{\boldsymbol{X}} = \boldsymbol{S\Lambda T^t}$, considering $\widetilde{\boldsymbol{X}} = \widetilde{\boldsymbol{U}}\widetilde{\boldsymbol{V}}^{\boldsymbol{t}}$ then there are two unmixing matrices $\boldsymbol{W_s}$ and $\boldsymbol{W_T}$, and $\widetilde{\boldsymbol{U}} = \boldsymbol{SA_S}$, $\widetilde{\boldsymbol{V}} = \boldsymbol{TA_T}$, thus $\widetilde{\boldsymbol{X}}$ can be written as:

$$\widetilde{\boldsymbol{X}} = \boldsymbol{S\Lambda T^t} = \widetilde{\boldsymbol{U}}\boldsymbol{W_S}(\widetilde{\boldsymbol{V}}\boldsymbol{w_T})^{\boldsymbol{t}} = \widetilde{\boldsymbol{U}}\boldsymbol{W_S}\boldsymbol{W_T^t}\widetilde{\boldsymbol{V}}^{\boldsymbol{t}} \tag{3.18}$$

In Antarctica, the mass change is highly related to the spatial distribution of glaciers, and the impact of GIA is uncertain in spatial distribution and quantity. Therefore, we first decided to use spatial ICA in this study. The algorithm applied is provided by Stone and Porrill (1999).

3.2 Previous Research for Extraction Geophysical Signals

Various statistical methods have been introduced to analyze GRACE-derived signals, including PCA and ICA. (Schmidt et al., 2008; Schmeer et al., 2012; Talpe et al., 2017; Forootan and Kusche, 2012). ICA is known to effectively separate spatiotemporal GRACE-derived mass changes into independent components (Forootan and Kusche, 2012).

One disadvantage of PCA is that PCA extracts the primary components according to the variance distribution of a measured geophysical field, which always leads to the extraction of the stronger signals and the potential dismissal of relatively weak but highly independent signals. PCA-extracted features are statistically uncorrelated to each other, which means that signal mixing remains a problem (Cardoso, 1992). ICA takes a different approach to PCA in exploring a dataset by treating all of the components equally. The goal of ICA is to find a linear transformation that can decompose the observations into independent components using high-order statistics.

Forootan and Kusche (2012) were the first to employ ICA for GRACE data analysis. They conducted both PCA and ICA to analyze the simulated synthetic data, compared the results with real GRACE products, and found that the ICA results were closer to "optimal decomposition", which indicated that ICA may be a more suitable approach for solving the problem of unknown source signal decomposition. ICA has been successfully applied to various studies, including the separation of independent water storage patterns in the Nile sub-basins and their relationship to climate indices, such as El Niño Southern Oscillation (ENSO) and Indian Ocean Dipole (Awange et al., 2014). ICA was also

used to analyze the variations in various components of an Indian hydrological system (Banerjee and Kumar, 2018), derive the relationship between land water storage changes in Africa and global climate indices (Anyah et al., 2018), and determine the ICA-derived Glacial Isostatic Adjustment (GIA) uplift in Fennoscandia and Laurentia using GRACE data, which obtained comparable results to regional Global Positioning System (GPS) observations (Shafiei Joud et al., 2019).

Shi et al. (2022) also demonstrated that the GIA signal in the Antarctic can be extracted using ICA. The GIA-related pattern was qualitatively extracted and compared with existing GIA models, showing a high level of correlation in spatial distribution. The results highlight the utility of the ICA method for analyzing Antarctica mass changes and suggest that ICA may be a suitable approach for solving the uncertainty in the source signals and constraining the mixing pattern in Antarctica. This study builds upon the finding of Shi et al. (2022) in exploring further applications of the ICA method.

Chapter 4

ICA Analysis for GRACE/GRACE-FO and Satellite Altimeter

4.1 GRACE/GRACE-FO

4.1.1 Data

The GRACE/GRACE-FO Level-2 products are mainly provided by the three official data centers: the Jet Propulsion Laboratory (JPL), the Center for Space Research (CSR), and the German Research center for Geosciences (GFZ). This work used Release 06 productions of spherical harmonic (SH) coefficient, which includes all of the available GRACE/GRACE-FO data between April 2002 and June 2020 except for a data gap from July 2017 to June 2018.

Discrepancies exist among the datasets offered by the different data centers. These may be consequences of distinct processing applied by each center. To prevent any dataset bias, the SH coefficients were averaged from the three datasets to generate our input data. A detailed discussion of these discrepancies is present in Chapter.6.1.2.

Standard post-processing techniques were utilized for all SH coefficients included in this work. C20 replacement was used for both GRACE and GRACE-FO solutions, while C30 replacement was implemented only for the GRACE-FO solutions by employing coefficients obtained from satellite laser ranging suggested by the Goddard Space Flight Center(Loomis et al., 2020). The SH coefficients were truncated up to 60 order and

degree to decrease high-frequency noise. Additionally, a DDK4 filter was employed for smoothing (Kusche et al., 2009). Although there is an approximately one-year gap between the two missions, Velicogna et al. (2020) have demonstrated that the GRACE and GRACE-FO time series can line up well across the data gap in Antarctica. The final year of data obtained before the end of the GRACE mission (July 2016-July 2017) was not used due to deteriorating observations. Since ICA analysis can deal with data continuity issues, there is no need to fill the missing months and two-year gap (July 2016–May 2018) in the time series. Notably, as an important original signal, GIA was not given special treatment by any model in this study.

4.1.2 Results

PCA is used as a pretreatment for centering and dimension reduction. The first six principal components, which account for over 70% of the total variance, are selected as the inputs for ICA in this study. sICA will produce spatially independent modes over the study region, and their corresponding time series should exhibit the temporal characteristics of separate sub-regions. Fig. 4.1 shows the results of the first six ICA-extracted spatial modes, with their corresponding time series (IC1, IC2, IC3,..., IC6) given in Fig. 4.2. All of the temporal modes are normalized in this study.

Long-term Trend

There are three long-term components, Mode-1, Mode-2, and Mode-3, among the six ICs. Mode-1 spatial pattern (Fig. 4.1a) is very similar to the regression trend (Fig. 1.1), and its corresponding time series (IC1) shows a clear linear trend. Mode-1 mass changes are primarily distributed across the well-known glacier regions such as the large mass loss in the AMS and Bellingshausen Sea Sector, West Antarctica, mass loss in WL, and mass gain across DML and EL, East Antarctica.

However, some subtle differences may suggest potentially different meanings of the Mode-1 signal. The mass loss signal in the WL region is significantly spatially wider than the regression signal, which may be an indicator of basal melting along the Totten glaciers in this region. A comparison with the Bedmap2 bed topography (Fretwell et al., 2013)

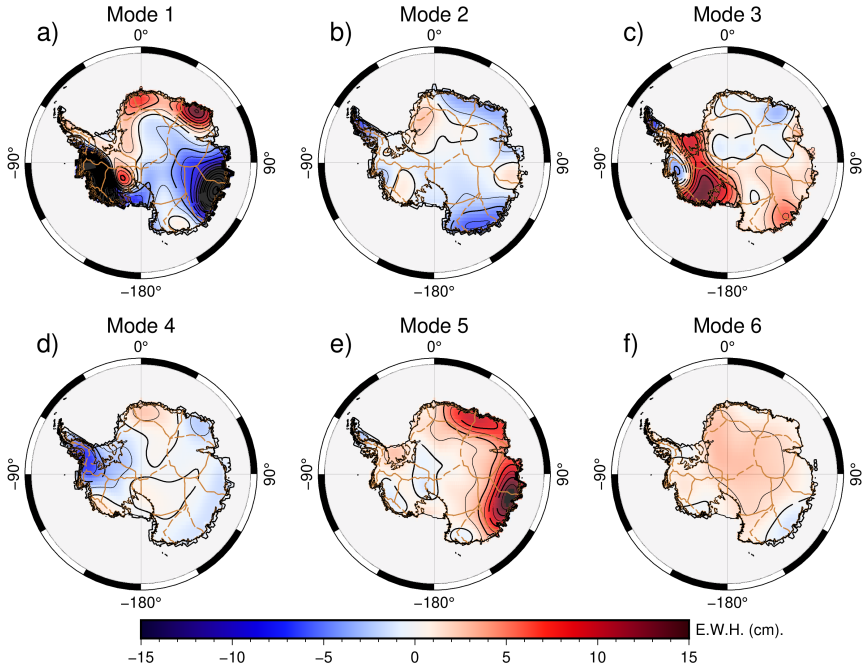

Figure 4.1: The first six ICA-extracted spatial modes for the entire study period.

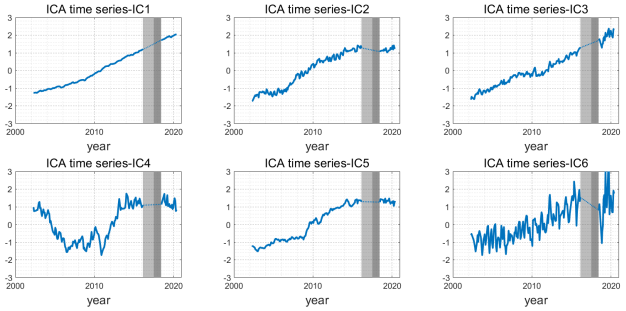

Figure 4.2: Time series of the decomposed spatial modes in Fig. 4.1. The shaded areas indicate the data gaps during the study period. The GRACE/GRACE-FO gap (July 2017–May 2018) is shown in dark gray, while the discarded period (July 2016–July 2017) is shown in light gray.

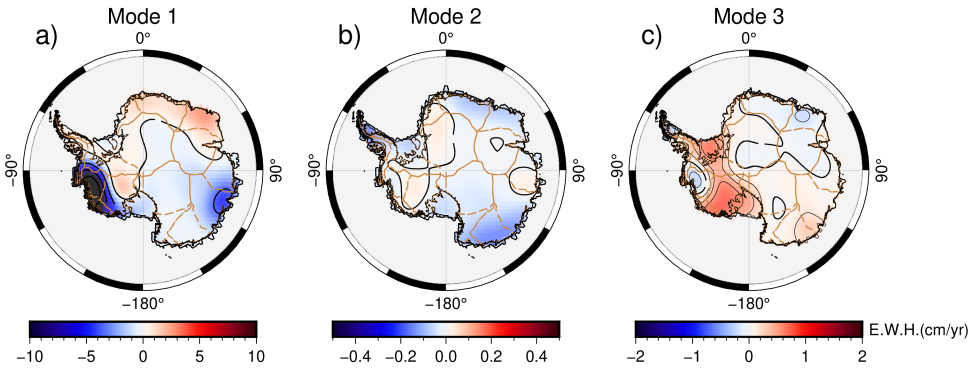

Figure 4.3: Rate maps of the trend components (Mode-1, Mode-2 and Mode-3) in Fig. 4.1. The corresponding time series are first simplified into linear trends. Then, the scale factors of the spatial vector are estimated by normalizing the resulting time series.

revealed that the mass-reducing area coincided with the deepest bed topography in this region. Hirano et al. (2021) indicated that the potential basal melting along Totten Glacier was caused by relatively warm Circumpolar Deep Water transport. Despite the risk of instability due to the regional bed topography, this sector remains in a stable state (Morlighem et al., 2020). Therefore, it may reveal a possible connection between the observed mass loss and the bed topography. Furthermore, the northern tip of the AP, which is dominated by strong seasonal changes, is not included in the Mode-1 signal. The RIS also shows a negative trend where the AIS mass loss is overwhelmed by GIA and a positive trend in the regression trend with no GIA correction. The above details suggest that the Mode-1 signal can be largely attributed to glacier changes.

The Mode-2 captures information on the glaciers that are not captured by the Mode-1. This signal, in combination with its corresponding time series, IC2, indicates that these regions are in a relatively balanced state between 2002 and 2006, and then experience mass loss after 2006. The same temporal evolution of AIS mass change has been observed in recent satellite altimetry studies (e.g., basin J"–K and D–D' in Schröder et al. (2019)).

The Mode-3 signal is the other long-term component, and its mass gain region is primarily localized across the interior ice plateau of MBL and also the RIS, where it is greatly affected by GIA. The Mode-3 spatial distribution is very similar to many GIA models. The long-term trend can still be clearly obtained, even though the mixing of some periodic

signals, such as the northern tip of the AP, leads to jaggedness in the IC3 time series.

Periodic Components

ICA also effectively separates the periodic components from the long-term components. Time series IC4 and IC6 show periodic signals on different time scales. Mode-4 signal captures the mass loss along the west coast of the AP, which is concentrated along the larger glaciers (e.g., George VI). The corresponding IC4 time series shows periodic signals at the 3–4-yr scale, which is probably related to periodic atmospheric and oceanic changes around Antarctica. Mode-6 signal shows mass gain that is distributed across the entire AIS, with the corresponding IC6 time series possessing a cyclical signal with a period of one year. Mode-6 signal may be related to seasonal changes across Antarctica. Mode-4 and Mode-6 signals demonstrate that ICA can effectively separate periodic meteorological signals and long-term signals.

Independent Events

ICA can also identify accidental independent events. In Mode-5 it can be found that there were two significant mass gain signals in East Antarctica, with the largest mass gain occurring in 2009 and the other in 2011. The temporal coincidence of these signals with the two extreme snowfall events in 2009 and 2011 that were reported by Boening et al. (2012) suggest a direct connection between the Mode-5 signal and snowfall events. The influence of anomalous snowfall events can also be found in other cyclical IC4 components. The strange variations around 2009 are considered to be driven by snowfall events.

4.2 Altimeter

The altimeter dataset from Schröder et al. (2019) is used in this section, which contains multi-satellite data including Seasat, Geosat, ERS-1, ERS-2, Envisat, ICESat and CryoSat2. Bias and other errors have been well-treated after a series of post-processing. It is provided in the form of consistent monthly grid data. Time period from 2000 to 2019 is selected here for comparing with GRACE/GRACE-FO.

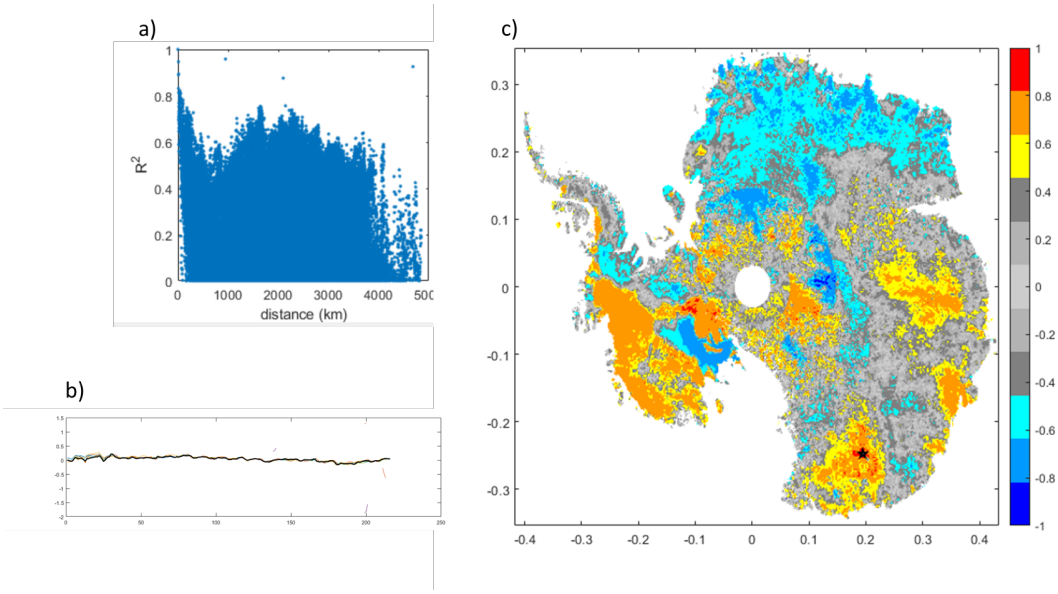

Figure 4.4: (a) Distribution of correlation coefficients as distance increases; (b) Time series of the ten grids with the highest correlation coefficients to the reference point; (c) Correlation coefficients map with a star marking the location of the reference point.

4.2.1 Re-sampling and Error Estimating

This section presents an analysis of the spatial autocorrelation of the altimeter data and attempts to determine an appropriate re-sampling method for generating a dataset with a spatial resolution comparable to GRACE/GRACE-FO for the purpose of direct comparison.

Each grid in the geophysical field is not always independent, sometimes it is artificially segmented in the generation of the dataset (as in the case of GRACE Mascon products). On the other hand, the variation of a given point within a certain spatial extent always has a higher correlation with neighboring points compared to distant points since the nearby area are always controlled by similar physical processes. Therefore, this kind of spatial auto-correlation is analyzed here to evaluate an appropriate resampling strategy. As an example, a point in EA is selected here. Its time series is compared with all other points in Antarctica by calculating correlation coefficients, the result can be presented in Fig. 4.4. Based on the results presented in Figure 4.4, it is clear that (a) within the range of $< \mathbf{700; \boldsymbol{km}}$, the reference point exhibits a high correlation with the surrounding

points, and the correlation coefficient decreases as the distance increases, and (b) the points with the highest correlation coefficients are nearly identical.

In addition to traditional re-sampling, another strategy for reducing spatial resolution is to expand grid data into a SH basis and truncate it to a specific degree to eliminate high-frequency signals. This approach offers several advantages: first, using the same representation as the gravity field data makes the two datasets more comparable; second, given the study's focus on the entire AIS, using SH expansion can more effective in continental scale. The altimeter data have a very high spatial resolution, and considering the native resolution of GRACE/GRACE-FO, at least 60 orders (300 km) is required to ensure the consistency of two different datasets. In this study, a conventional **1** spatial grid is used, which requires a higher truncation degree. The coefficients obtained after expansion are then transformed into a spatial grid.

The elevation data is expanded using SH functions and truncated to 90 and 120 degrees, respectively. For each grid, the root mean square (RMS) of the time series obtained by traditional resampling and SH expansion is calculated. The test is performed on a **1** spatial grid, which is higher than the native resolution of 90 and 120-degree expansions. Therefore, the coefficients are not truncated to the same 60-degree as the gravity field. As shown in Figure 4.5, the elevation data derived from the 90-degree expansion exhibits significantly larger RMS errors than the 120-degree expansion, particularly in coastal regions. As ICA is recommended to be performed on spatial grid (see Sec.6.2.2)ï¼$\frac{\mathbf{1}}{\mathbf{4}}$due to the truncation errors, SH expansion did not exhibit significant advantages over traditional resampling. Consequently, traditional resampling is used conservatively for the next step of the ICA analysis in this study. However, properly integrating the altimetric data requires further investigation of truncation errors, signal leakage, and observation errors in coastal regions.

4.2.2 Results

In this section, the exact same analysis as Sec.4.1.2 is applied to the re-sampled altimeter data obtained in Sec. 4.2.1. In this study, both altimetry data and GRACE/GRACE-FO data are unified into a one-degree grid. For GRACE/GRACE-FO it requires an

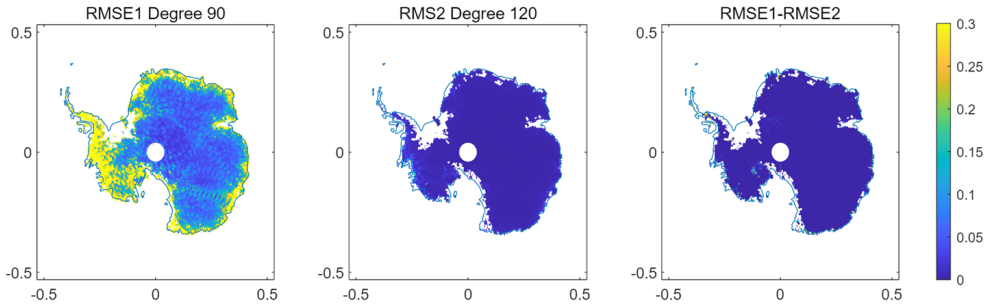

Figure 4.5: Comparison of traditional resampling and SH expansion of altimetry data. The RMS of SH expansion and traditional resampling time series is calculated for each grid. RMS1 and RMS2 correspond to 90-degree and 120-degree expansions, respectively.

interpolation through which no information will be lost. But for altimetry data, it is a different case. Reducing the native resolution will inevitably lead to the loss of high frequency information that can affect ICA results directly. Another result of the high native resolution is a lower variance contribution ratio for the same principal component number. The accumulated eigenvalue spectrum for altimetry and GRACE/GRACE-FO is plotted in Fig. 4.6. In the pretreatment of PCA, when using the same truncation number of **6** as GRACE/GRACE-FO the accumulated eigenvalue of altimetry is less than **0.5** much less than the value of **0.75** for GRACE/GRACE-FO.

Compared to GRACE/GRACE-FO, the ICA analysis of altimetry data is more complex. On the one hand, high-frequency signals require more components to describe detailed information. On the other hand, altimetry data is more sensitive to surface physical processes and less sensitive to changes in the solid Earth, making it impossible to establish one-to-one correspondence with the modes of GRACE/GRACE-FO data. The results of the first six spatial modes extracted using sICA, along with their corresponding time series, are shown in Fig. 4.7 and Fig. 4.8, respectively. All of the temporal modes are normalized in this section.

Long-term Trend

IC1 and IC3 can be recognized as two long-term components among the six ICs. The spatial distribution of Mode-1 is highly consistent with that of GRACE/GRACE-FO

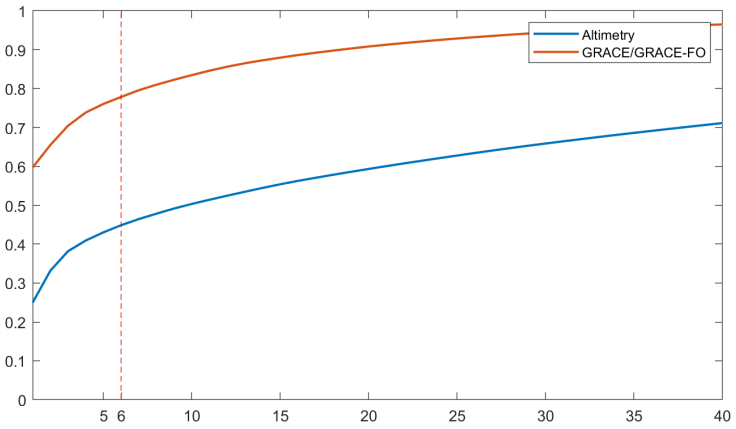

Figure 4.6: Accumulated eigenvalue spectrum for altimetry and GRACE/GRACE-FO.

(Fig. 4.1a). A similar region with decreasing trend can be found in glacier regions such as AMS and Bellingshausen Sea Sector. Increasing regions across DML and EL, are also in good agreement. The differences can be found primarily in some areas like MBL, where the surface elevation is decreasing, but the GRACE results reveal an increasing trend in the interior part of this region. In addition, the elevation of GVL is decreasing, but there is no significant decreasing trend in mass changes. These differences may be caused by non-surface processes.

IC3 represents another long-term trend, but it is not a constant trend, and a turning point can be found around 2011. The increasing region in Mode-3 is localized across the MBL and GVL, while the decreasing region is concentrated in AMS and WL. An important difference is that IC3 is not a constant linear trend, which distinguishes it from the altimetry component of GRACE/GRACE-FO.

Consistent with expectation, no significant GIA signal is separated using altimetry data, as GIA will exhibit another long-term component. This may be attributed to the low signal-to-noise ratio of GIA. The maximum of GIA uplift is typically on the order of a few millimeters per year, which is two orders of magnitude smaller than the annual glacier thinning of several meters.

Periodic Components

The high-frequency information contained in altimetry data may lead to more periodic components in ICA results. Time series IC2, IC3, and IC6 show periodic signals on different time scales, which may be related to the interannual variability of the SMB. Similar evidence can be found in some studies of SMB, for example, Kim et al. (2020) used PCA to extract three principle modes of SMB, showing the periodicity of SMB at three different time scales. It can be found that the IC2 and Mode-2 are highly similar to second mode of SMB. Therefore, it can be speculated that the periodicity in altimetry data is more closely related to the SMB process.

Independent Events

Coincidentally, the snow accumulation due to extreme snowfall events is also separated in altimetry results. The time series IC5 increases rapidly around 2010, its corresponding spatial distribution Mode-5 shows that not only the snowfall area of East Antarctica is contained but also other coastal regions are included. This could be largely attributed to incomplete decomposition.

In general, the ICA results from altimetry data are not as clear and straightforward as those from GRACE/GRACE-FO. This difference is to be expected, considering two reasons: the first is the low contribution ratio of the input data to the total variance, and the second is that the high-frequency information contained in altimetry data reflects very local physical processes which may be difficult to separate. However, the ICA results from altimetry data still provide us with valuable information as a complement to GRACE/GRACE-FO results. The spatial distribution is comparable in some common modes that reflect signals such as glacier melting and snowfall. This indicates that the ICA results are not only statistically but also physically meaningful, as comparable results were obtained even with completely different types of observations.

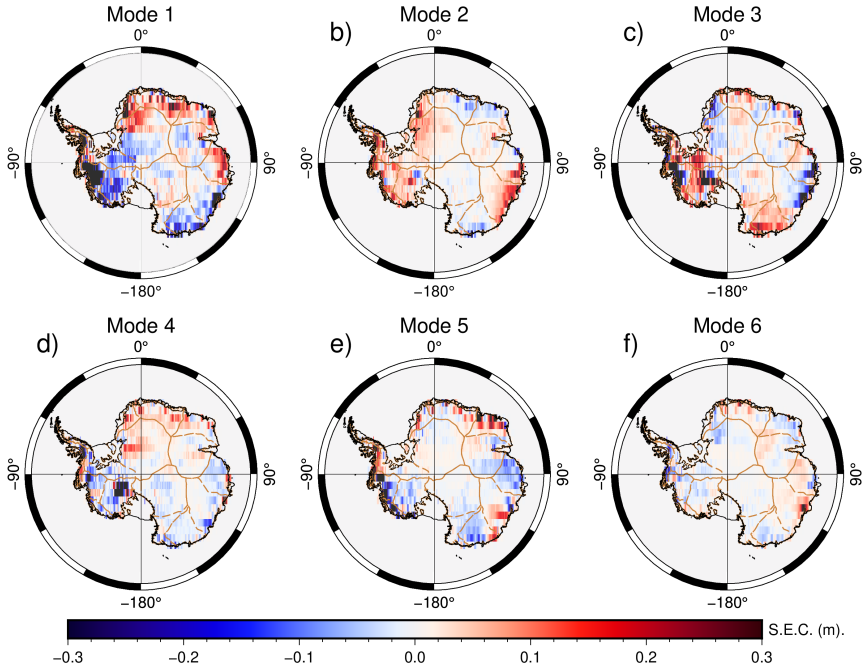

Figure 4.7: The first six spatial modes extracted by sICA for altimeter data.

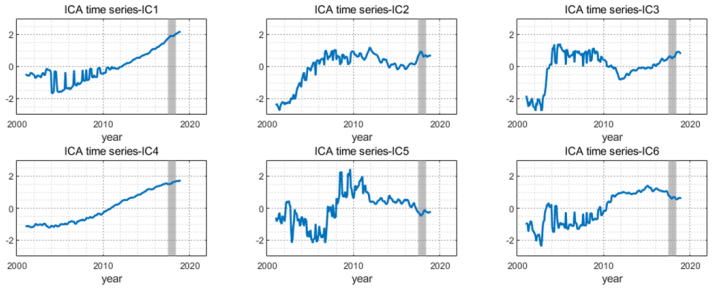

Figure 4.8: Corresponding time-series of the decomposed spatial modes in Fig. 4.7.

Chapter 5

Model and Regional Study

5.1 GIA Model

To better understand the ICA results, it is necessary to investigate their physical meaning further. In this chapter, we examine the GIA-related modes separated by ICA using forward GIA models. Additionally, we conduct a detailed investigation of the AIS drainage basins, primarily introducing an SMB model to analyze the physical processes in each basin. This approach provides further insight into the physical interpretation of each mode.

This section estimates rate maps for the three trend components mentioned above, as shown in Fig. 4.3. Mode-1 possesses the same order of magnitude as the regression trend, and Mode-2 and Mode-3 are one order of magnitude smaller in comparison.

Furthermore, the spatial correlation coefficient (SCC) is used as a measure of the agreement between two spatial signals, as in Boergens et al. (2014):

$$\boldsymbol{SCC} = \frac{\sum_{j=1}^{N} \boldsymbol{ref_s}(j) \cdot \boldsymbol{res_s}(j)}{\sqrt{\sum_{j=1}^{N} \boldsymbol{ref_s}(j)^2 \cdot \boldsymbol{res_s}(j)^2}}, \tag{5.1}$$

where $\boldsymbol{ref_s}$ is the reference signal and $\boldsymbol{ref_s}$ is the separated signal, which consists of $\boldsymbol{N}$ grid points. The SCCs between the Mode-3, and four GIA models: A (2013), ICE-6G, W12 and IJ05_R2 are calculated (Geruo et al., 2013; Peltier et al., 2018; Whitehouse et al., 2012; Ivins et al., 2013) (Fig. 5.1). The results are shown in Table 5.1. Mode-3 has the highest SCC with ICE-6G and the lowest SCC with IJ05_R2, which implies a moderate-to-strong correlation between the Mode-3 signal and the GIA effect. Com-

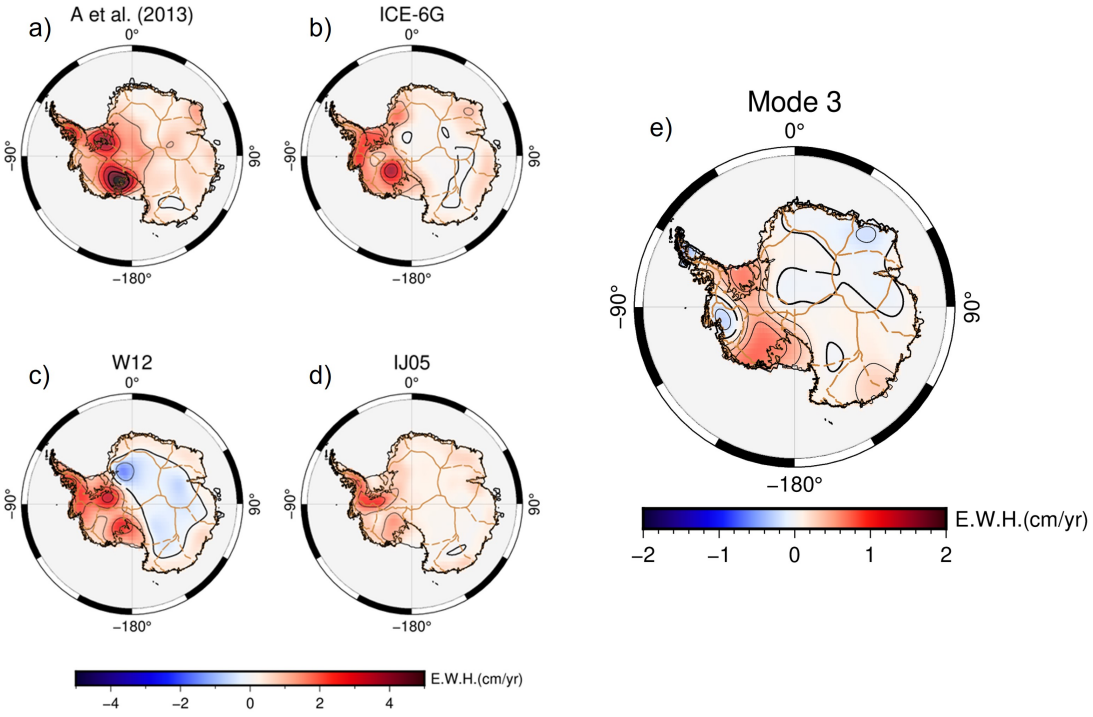

Figure 5.1: Comparison of GIA models and ICA-extracted GIA. a)–d) are annual rate of GIA effects in E.W.H.(cm) derived from four GIA forward models, e) is Mode-3 extracted from GRACE/GRACE-FO in Fig. 4.1.

paring the SCC of 0.7023 between the ICE-5G and ICE-6G, it is reasonable to infer that Mode-3 may reflect the GIA signal. The variance ratios ($\frac{\boldsymbol{Var(Model)}}{\boldsymbol{Var(Mode-3)}}$) are also calculated for quantitative comparison, Mode-3 is quantitatively several times smaller than forward models. It can also be found that the strongest GIA effect is derived by A (2013), which suggests up to 5.64 times larger than Mode-3 in quantity, while the weakest IJ05_R2 suggests a comparable uplift with Mode-3. The results implied a relatively low upper-mantle viscosity as suggested by IJ05_R2 ($\boldsymbol{0.2 \times 10^{21}\ Pa\ s}$). Another possible explanation is the incomplete decomposition of the ICA method as some portion of the GIA effect still remains in other linear components resulting in small amplitude values for the separated GIA mode. Nonetheless, the spatial distribution of the separated GIA mode appears stable, and this observation can further contribute towards constraining the ice history.

Table 5.1: Spatial correlation coefficients and amplitude ratios between the GIA models and ICA spatial modes (95 percent confidence level).

	Correlation coefficient	**Variance Ratio (Model/ICA mode)**
A et al. (GeruoA et al., 2013)	0.710	5.640
ICE-6G (Peltier et al., 2018)	0.720	2.487
W12 (Whitehouse et al., 2012)	0.620	3.366
IJ05_R2 (Ivins E.R. et al., 2005)	0.544	1.007

5.2 Mass Balance for Regional Drainage Basin

AIS is divided into Western Antarctica Ice Sheet (WAIS), Eastern Antarctica Ice Sheet (EAIS), and Antarctica Peninsula (AP) based on historical definitions, and can be further separated into multiple drainage basins based on modern Digital Elevation Model (DEM) information and ice velocity data. The conventional basins from Rignot et al. (2013) is used in this study (Fig. 5.2.1). This chapter will investigate the mass and volume changes of each Antarctic basin. A SMB model SMB–NHM (庭野匡思 et al., 2021) will be introduced, plus the observation data from GRACE/GRACE-FO and satellite altimeters, and combined with ICA results for further understanding the physical sources of AIS changes.

5.2.1 Classification of Antarctica Drainage Basins

The mass changes in each basin may have a more distinct dominant physical signal when compared to the whole AIS. Some basins may be dominated by ice dynamics, some others may be strongly affected by seasonal meteorological processes. The different sensitivities of the elevation and gravity fields to the same physical process are fundamental to distinguish these processes. The average mass variation of each basin is estimated by the SMB model and GRACE/GRACE-FO, respectively, and the average surface elevation variation is estimated by the altimeter observation. Dimensionless time series was obtained by taking the average of all points within the basin and standardizing the time series, and for SMB time series, its trend was specially removed. The results are shown in Fig. 5.2.1.

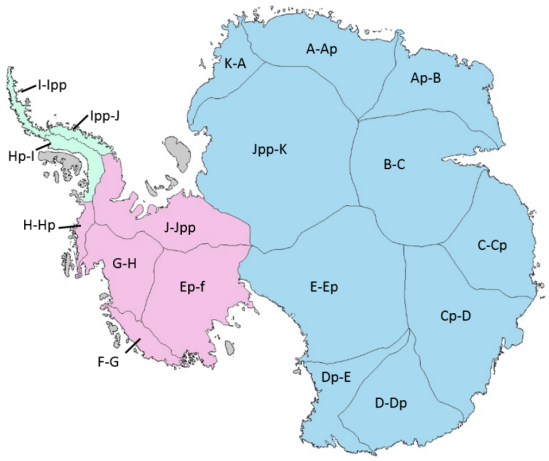

Figure 5.2: Boundary and definitions of Antarctica drainage basin from Rignot et al. (2013). The blue-colored region is EAIS, the pink-colored region is WAIS, and the green-colored region is AP.
(http://imbie.org/imbie-2016/drainage-basins/))

All basins can be classified into four groups based on the movements of three kinds of data (see Fig. 5.2.1 and Table.5.2.1). Type-I, the time series of all three are reconciled with each other. Type-II, one of three kinds of data is inconsistent with others, which can be further divided into 3 sub-types. Type-II-a, discrepancy in altimeter, II-b discrepancy in SMB, and II-c discrepancy in GRACE/GEACE-FO. Type-III is that all time series are not consistent with each other or hard to be classified.

Type I

In Type-I basins, the mass variations estimated by the SMB model coincide with the observed total mass change. The volume change is synchronized with mass change, suggesting that almost all mass changes within the basin result from SMB processes and mainly occur on the surface of the AIS. The stability of the long-term trend indicates that the glaciers within the basin tend to be stable, with no noticeable acceleration or deceleration in flow speed.

Basins Cp-D, Dp-E, and Hp-I are considered to be Type-I basins. All Type-I basins show a good agreement in trend for three time series. But there are still some subtle

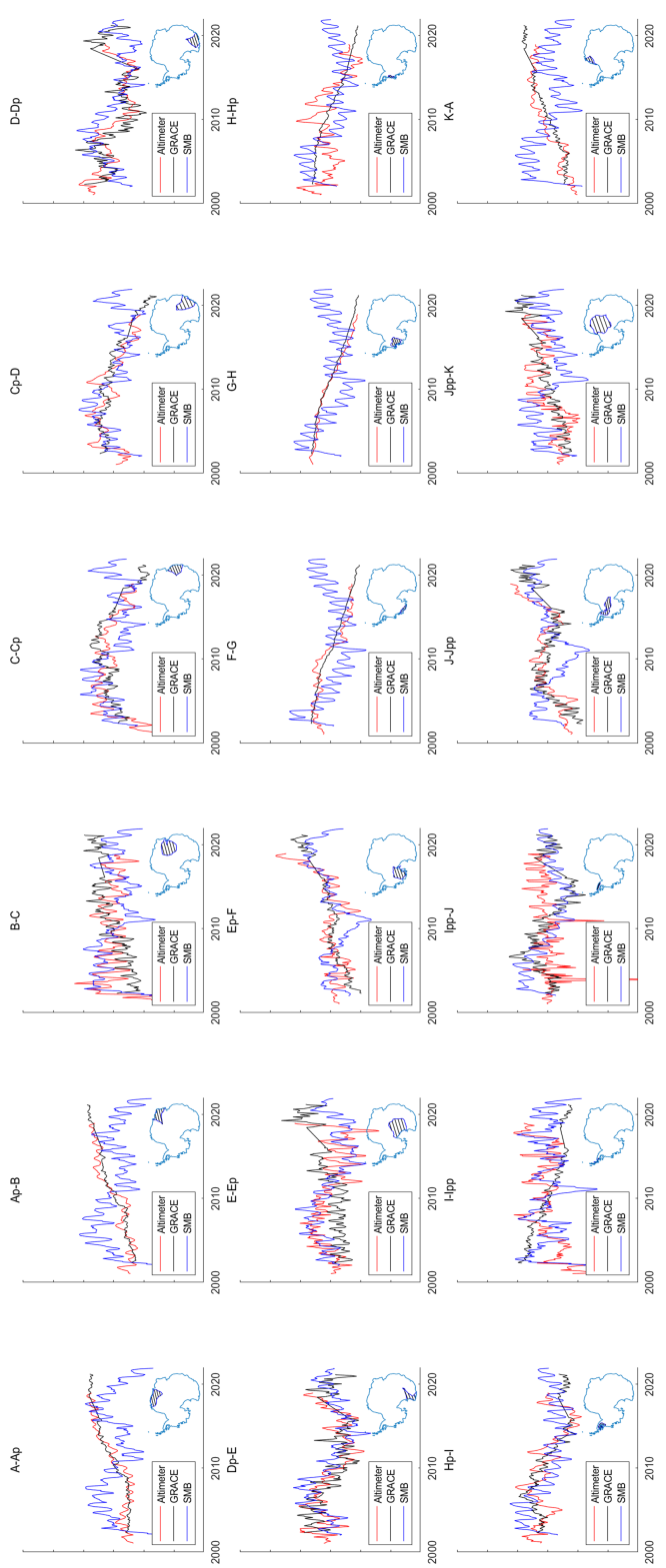

Figure 5.3: Mass and elevation changes of drainage basins based on Rignot et al. (2013). The elevation change measured by satellite altimeters, and the average mass changes derived by GRACE/GRACE-FO and SMB model are plotted in black, red, and blue lines respectively. Taking the average value of each drainage basin and normalizing the resulting time series to be dimensionless.

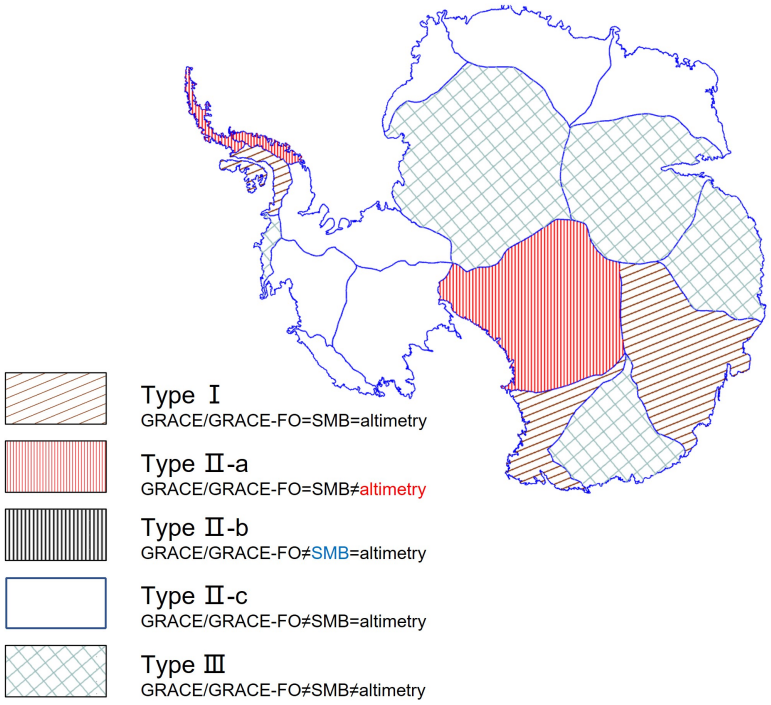

Figure 5.4: Classification of the Antarctic drainage basins.

Table 5.2: Classification of Antarctic basins based on GRACE/GRACE-FO mass change, surface elevation, and SMB change characteristics.

Type		Basin	Region	Description
I		Cp-D	East	GRACE/GRACE-FO = SMB = altimetry
		Dp-E	East	
		Hp-I	Peninsula	
II	a	Ipp-J	Peninsula	GRACE/GRACE-FO = SMB ≠ altimetry
	b	A-Ap	East	GRACE/GRACE-FO ≠ SMB = altimetry
		Ap-B	East	
		F-G	West	
		G-H	West	
		K-A	East	
	c	E-Ep	East	GRACE/GRACE-FO ≠ SMB = altimetry
		I-Ipp	Peninsula	
III		B-C	East	GRACE/GRACE-FO ≠ SMB ≠altimetry
		C-Cp	East	
		D-Dp	East	
		Ep-F	West	
		H-Hp	West	
		J-Jpp	West	
		Jpp-K	East	

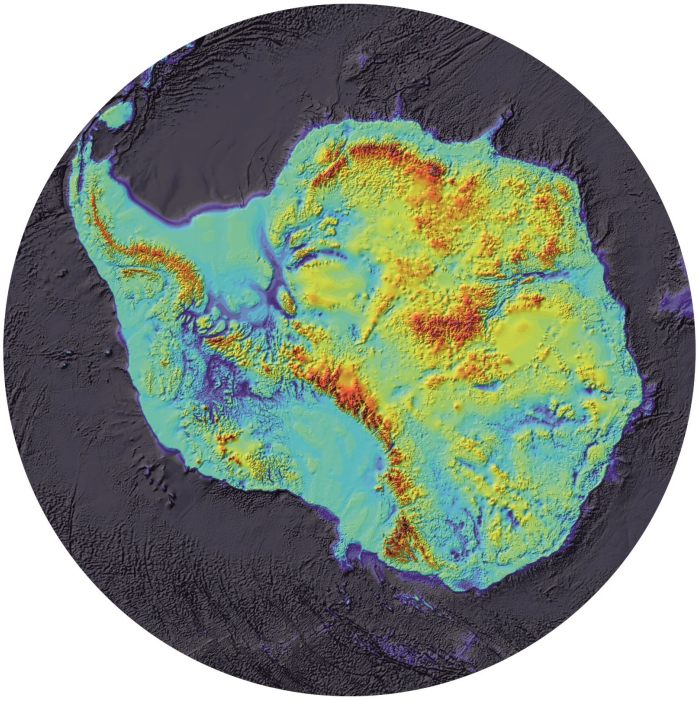

Figure 5.5: Bed elevation for Antarctica (Fretwell et al., 2013)

differences, in Hp-I the periodic variations are more pronounced in the SMB and altimetry time series.

Combining with subglacial bed elevation information, for example comparing with Bedmap2 as shown in Fig. 5.2.1 (Fretwell et al., 2013), it can be found that the coastal area of Type I basins is localized in high elevations and lacks potential for further access to the ocean, excpet for Cp-D. Totten Glacier in Cp-D is localized in deep ground that possible for direct contact with warm ocean. A longer period of data is still needed for confirmation.

Type II

Type II-a

In Type-II-a basins where the mass changes can be well estimated with the SMB model but are not consistent with surface elevation changes, which suggests that mass changes

may largely be attributed to SMB, while the change in ice sheet volume barely affects the mass changes.

II-a is not a very common type of basin in Antarctica, Ipp-J is the only basin that can be classified, whereas the most negative SMB can be found. Models simulation also suggests that this basin is dominated by meteorological factors. This phenomenon is quite unusual, as it is difficult to imagine the SMB process deviates that much from the altimetry changes. One possible explanation for the phenomenon is the error in the altimetry observation. Schröder et al. (2019) also reported the significant uncertainty in this basin.

Type II-b

In Type-II-b basins, the GRACE mass changes have the same trend with elevation changes but have discrepancies with SMB. The gap between SMB and observations could be caused by the ice dynamics because the changing in glaciers contribute to total mass changes that are not included in SMB model. It could also be caused by inappropriate model estimation.

Type-II-b is the most common type of basin in Antarctica. A-Ap and Ap-B are two typical II-b basins. They are characterized by the scissor-shaped difference that appeared around 2010 when time series of altimeter and GRACE mass is increasing rapidly, but SMB shows no significant increase. The mass increase is contributed by snowfall events as mentioned in Section.4.1.2, there are two extreme events in these two basins were reported by Boening et al. (2012). This could be due to the lack of capability in simulating extreme events or inappropriate removal of the trend term in the SMB time series.

In some basins with long-term mass reduction, the situation will be different. For example, basins F-G and G-H, a clear long-term mass loss is observed by GRACE, accompanied by an elevation decrease. However, the SMB model suggests that there is no clear trend in the these basins and shows periodic fluctuations. The discrepancy indicates the strong ice discharge from glaciers in the region.

Type II-c

In Type-II-c basin, the SMB changes have a similar movement with elevation changes but have discrepancies with GRACE observations. This suggests almost elevation changes are contributed by SMB processes and imply no significant surface glacier acceleration. And the gap between altimetry and mass could be linked to some processes that do not occur on the AIS surface such as basal melting.
Long-term mass loss has been observed by GRACE for basin I-Ipp, which is located on the west coast of the AP. However, the surface elevation and SMB are primarily dominated by periodic signal, with no clear trend. This suggests the possibility of basal melting in I-Ipp.

Type III

Type-III basins are more complex, because each basin behaves differently. Some basins could show a pair of time series with opposite trends and the other takes the average of these two, while some could show a certain phase delay between the periodic time series. For H-Hp, the SMB does not show a clear trend while GRACE indicates a long-term mass reduction, unlike both above, altimetry time series presents a fluctuation of several year cycles which can be assumed that the altimeter periodicity is closely related to ocean circulation. The mass reduction trend in this basin cannot be fully explained by surface glacier thinning, so the gap suggests potential bottom melting.
For Jpp-K, both SMB and altimetry present distinct annual cycles, but in opposite phases. GRACE is just the average of the two, balancing out this difference. The reasons for the opposite phases is not clear and cloud be related to mass redistribution within the basin.

5.2.2 Comparing with ICA Results

This section will revisit the ICA results from GRACE/GRACE-FO (Fig. 4.1 and Fig. 4.2) to make further interpretations for each mode, based on the classification information. This section mainly focuses on the differences in altimeter and GRACE/GRACE-FO results, and long periods that are not well understood.

Firstly, it is clear to see that the shaded area of Mode-1 in both GRACE/GRACE-FO and altimetry is highly similar to the spatial distribution of Type II-b, except for Cp-D (the blank area in Fig. 5.2.1). This demonstrated indicates that Mode-1 is closely related to the dominant signal of glacier changes and snow accumulation.

Mode-4 of GRACE/GRACE-FO exhibits periodic changes at a 3- to 4-year scale, mainly concentrated in the J-Jpp basin. By comparing the SMB time series of J-Jpp, it can be observed that IC4 shows a consistent periodicity with it. Additionally, weaker signals of Mode-4 can also be found in Ap-B, D-D-Dp, and A-Ap basins. By comparing the SMB time series of these basins, it can be found that they exhibit similar periodic characteristics, which explains why ICA classifies these regions into the same component. Therefore, it could be confirmed that Mode-4 is related to the multi-year periodic component of SMB.

Chapter 6

Better Way to Drive ICA

The result obtained by ICA is the optimal result in statistics, but it may not necessarily reflect physical processes. Therefore, it is particularly important to use ICA appropriately for understanding the real. In this chapter, we will mainly discuss the impact of different factors on the results of ICA, including the time period of the input dataset, discrepancies caused by different data centers, and different ICA algorithms. And the stability of the results of ICA will be discussed based on these.

6.1 Factors related to ICA Results

6.1.1 Time Period

In this section, the impact of input time period is discussed. Here, the period of extreme snowfall events is removed to eliminate the impact of these events, and verify whether the remaining long-term ICA components, which should be temporally insensitive, can still be obtained. For this, we first removed January 2009–June 2010 period, then divided the remaining dataset into two sections, and finally repeat the ICA analysis for each section. The order of the ICA results may vary due to the different subintervals. We reordered the ICA results to align the components with similar information to those for the entire dataset since the order of the ICA results does not represent the significance of each component. Furthermore, the fact that the different subintervals contain different information inevitably means the results from different subintervals may not be well aligned. The results of the former period (2002–2009) are shown in Fig. 6.1, with the correspond-

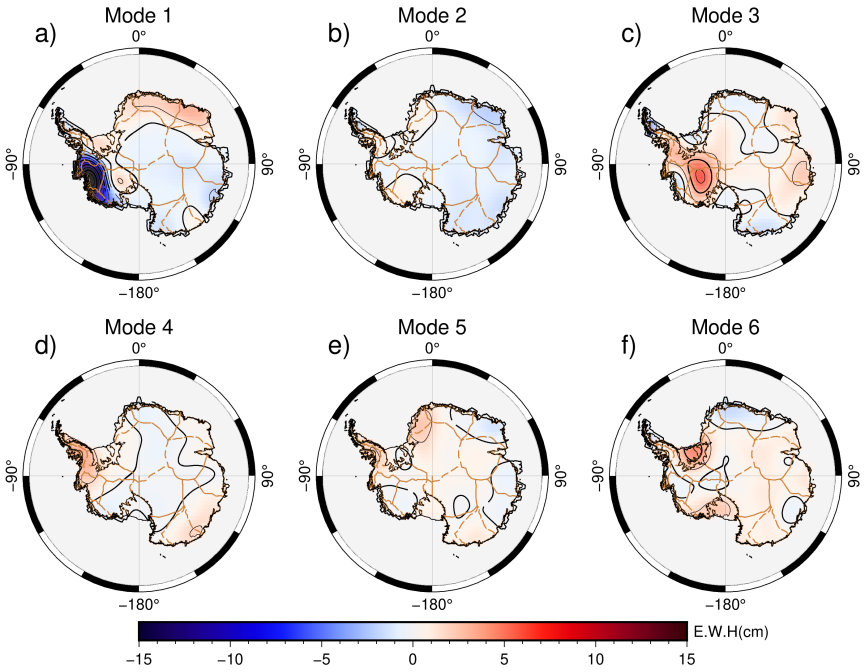

Figure 6.1: The first six ICA-extracted spatial modes for the former period (2002–2009).

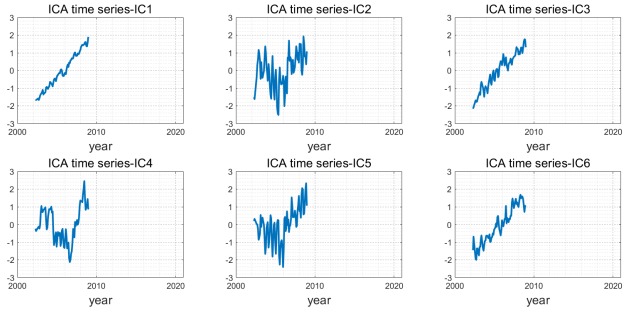

Figure 6.2: Corresponding time series of the decomposed spatial modes in Fig. 6.1.

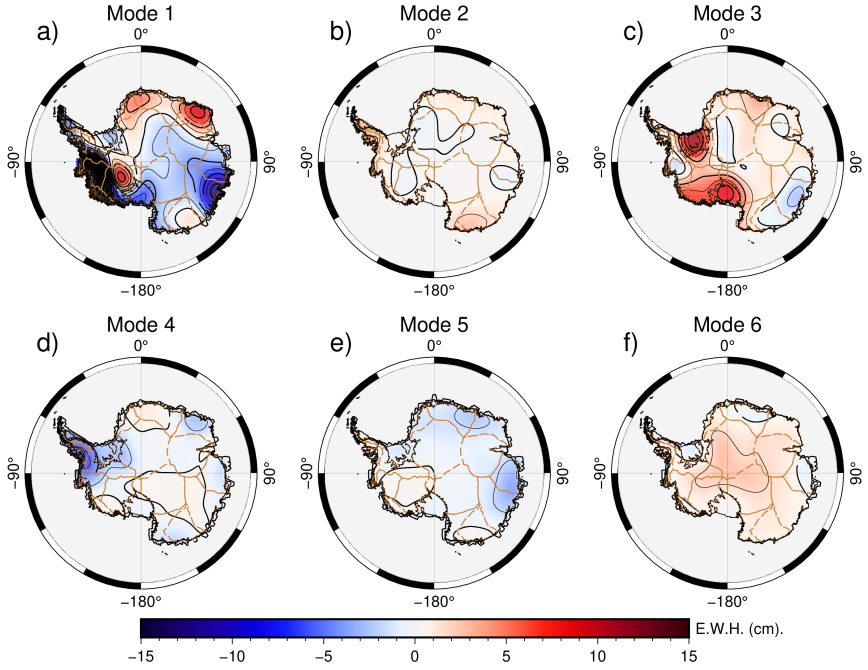

Figure 6.3: The first six ICA-extracted spatial modes for the latter period (2010–2020).

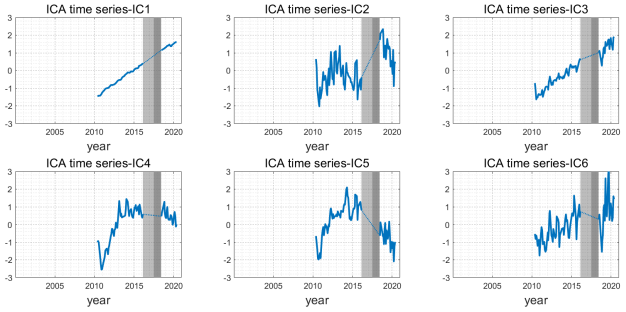

Figure 6.4: Corresponding time-series of the decomposed spatial modes in Fig. 6.3. The grey shading denotes the data gap in the study period, with the GRACE/GRACE-FO gap (July 2017-May 2018) in dark grey and the discarded period (July 2016-July 2017) in light grey.

ing time series presented in Fig. 6.2, and the results of the latter period (2010–2020) are shown in Fig. 6.3, with the corresponding time series presented in Fig. 6.4.

The mass gain component in East Antarctica (Mode-5 in Fig. 4.1), which is related to snowfall events, is no longer detectable in the results for the two periods after excluding the period of detected snowfall events, as expected.

A comparison of the results from the different time periods indicates that most of the basic spatial patterns of the long-term components (Mode-1 and Mode-3) have remained. The differences in their spatial distributions reflect the development of the same components at different periods.

Many interesting local differences are observed in Mode-1 glacial component. Some notable glacial changes that have occurred since 2009, such as the expansion of the West Antarctica mass loss area, the onset of significant mass loss along Totten Glacier, East Antarctica, and the onset of mass gain along Ice Stream C, West Antarctica, are identifiable (Fig. 6.3a).

The GIA-related modes for two time periods (Mode-3 in Figs 6.1 and 6.3) show significant spatial differences between the former and latter periods (Figs 6.1c and 6.3c), even though the GIA-related mode is still detectable across both time periods. The former is primarily concentrated across MBL, whereas the latter is primarily distributed across the RIS and FRIS. One potential explanation is the alteration of long-term trends for some glaciers associated with RIS around 2010, which makes it more difficult for ICA to separate the long-term changes of glaciers and GIA, and the shorter time span worsens the challenge.

We examine the SCCs between the ICA modes and GIA models (see Table 5.1) to determine the ability to extract the GIA signal via ICA. The results show that the SCCs for the GIA-related modes and ICE-6G is 0.624 for the former period, and 0.664 for the latter period, respectively. Considering that the SCC between the ICE-5G and ICE-6G GIA models is 0.7023, it is reasonable to infer that the two spatial patterns (single-peak and two-peak) may both reflect the GIA signal.

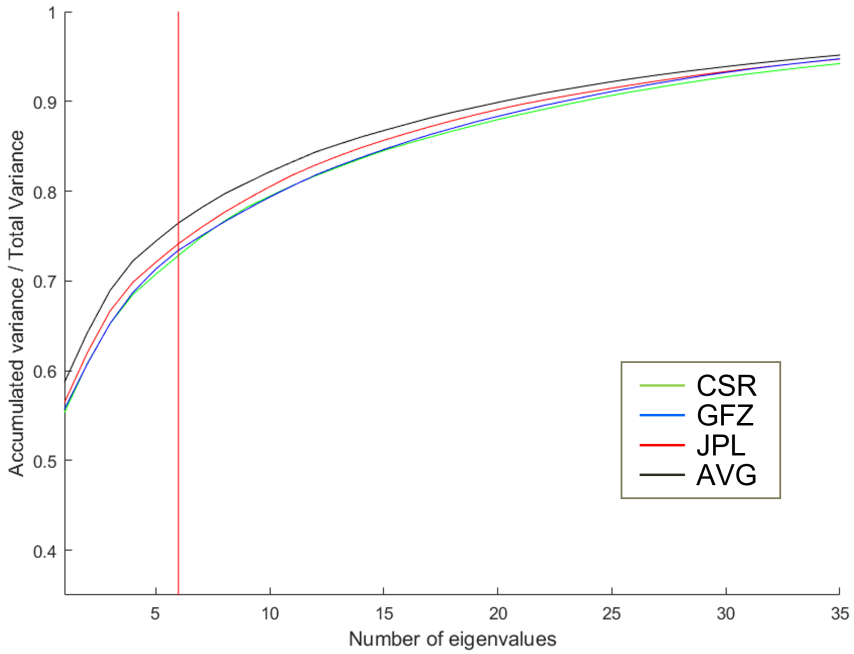

Figure 6.5: Accumulated eigenvalue spectrum derived from implementing PCA method on different datasets. Green, blue, red, and black curves are for the CSR, GFZ, JPL, and AVG (the average coefficients of the above three datasets) datasets, respectively. The red cutoff line indicates the first six eigenvalues that were selected.

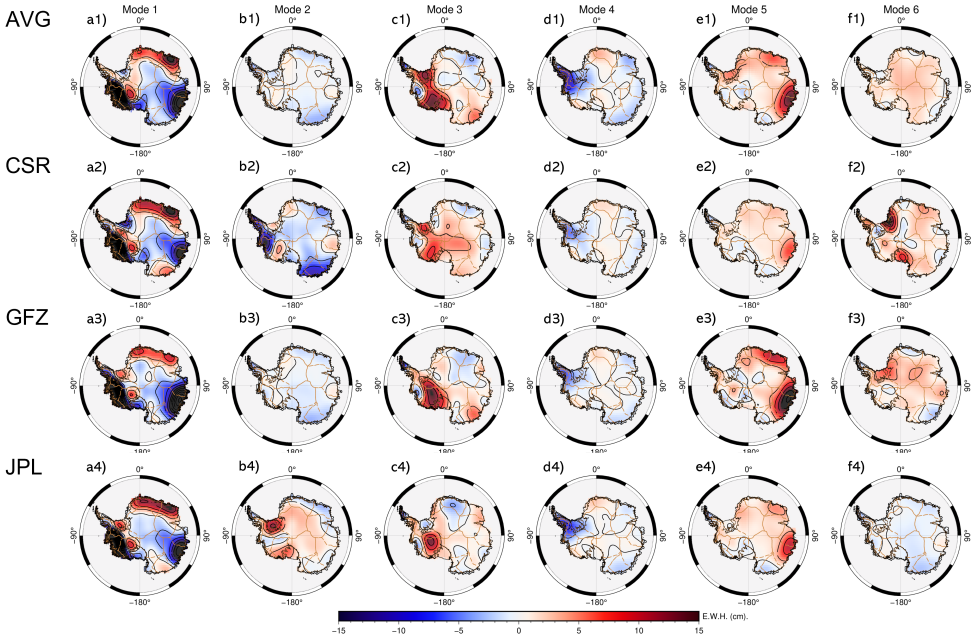

Figure 6.6: The first six spatial modes extracted via sICA from the AVG (average of three datasets), CSR, GFZ, and JPL datasets.

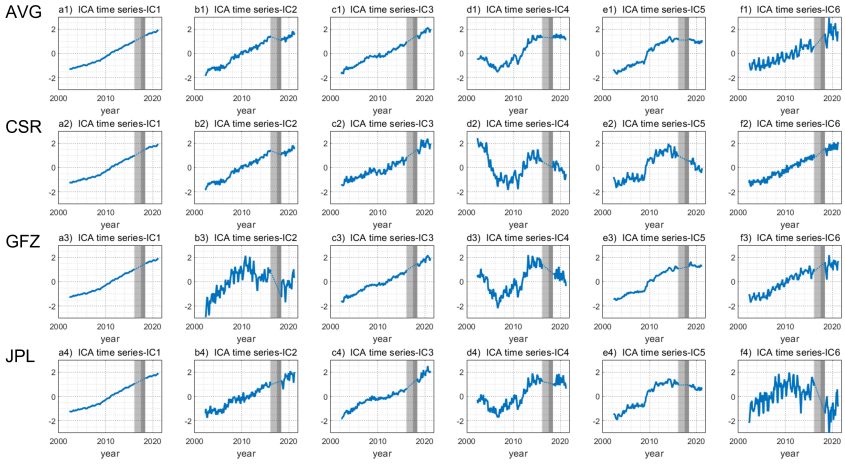

Figure 6.7: Corresponding time series of the decomposed spatial modes extracted via sICA from the AVG, CSR, GFZ and JPL in Fig. 6.6. The gray shading denotes the data gap in the study period, with the GRACE/GRACE-FO gap (July 2017-May 2018) in dark gray and the discarded period (July 2016-July 2017) in light gray.

6.1.2 Discrepancies between datasets

This study also tested the different spherical harmonic coefficients provided by three data centers (CSR, GFZ, and JPL) and their average. Firstly, calculate the eigenvector spectrum for each dataset via PCA (Fig. 6.5), which yielded accumulated variance ratio curves of the three individual datasets that were very similar. Each of the three datasets possess ratios above 0.7 for the first six components, with the JPL ratio being slightly higher than the other two, and the average (AVG) shows the highest ratios (even higher than that for each individual dataset), with a ratio of about 0.75.

Then employ sICA separately for the different datasets, with the results shown in Figs 6.6 and 6.7. We find that the results for the dominated ice/snow signals in Mode-1 are identical across the datasets. There is also a good agreement among the datasets for the periodic variations of the Antarctic Peninsula in Mode-4 and the snowfall events in Mode-5. However, there are different biases among each of the datasets for some of the weaker signals. For example, although the additional linear trends associated with the GIA signal have been successfully separated for all of the datasets (Figs 6.7 c1–c4), the corresponding spatial distributions differ widely (Figs 6.6 c1–c4). Among these, the AVG and CSR results show a two-peaked spatial feature across FRIS and MBL, respectively, whereas GFZ and JPL show a single-peaked spatial feature. Furthermore, the spatial distributions of the remaining high-frequency meteorological signals also differ significantly (Figs 6.6 f1–f4). This is potentially due to the large discrepancy in the minor signals after the PCA implementation in the first step. However, this could also be attributed to the signal mixing owing to incomplete decomposition. We therefore used the average solution of the three datasets, as mentioned in Sec.2, to avoid any bias in the results.

6.1.3 Comparison of Different ICA Methods and PCA

Different ICA methods can achieve different aspects of independence, as mentioned in Sec.3. sICA maximizes the independence in the spatial domain, while tICA maximizes the independence in the temporal domain. Different ICA methods may be suitable for

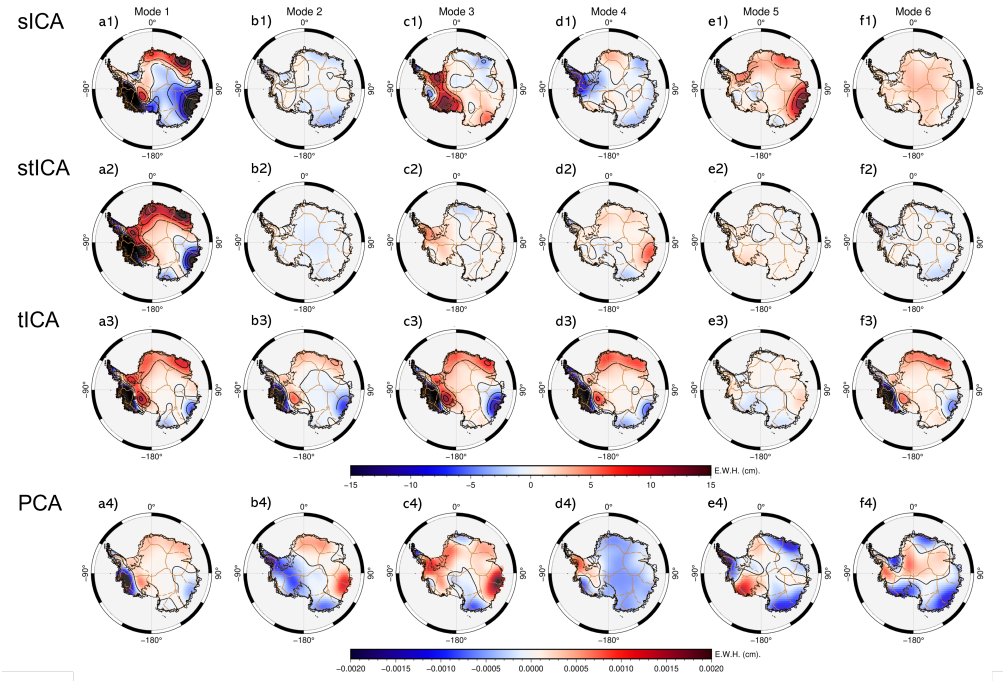

Figure 6.8: The first six spatial modes extracted via sICA, stICA, tICA, and PCA. Note the different color scales for the ICA and PCA results.

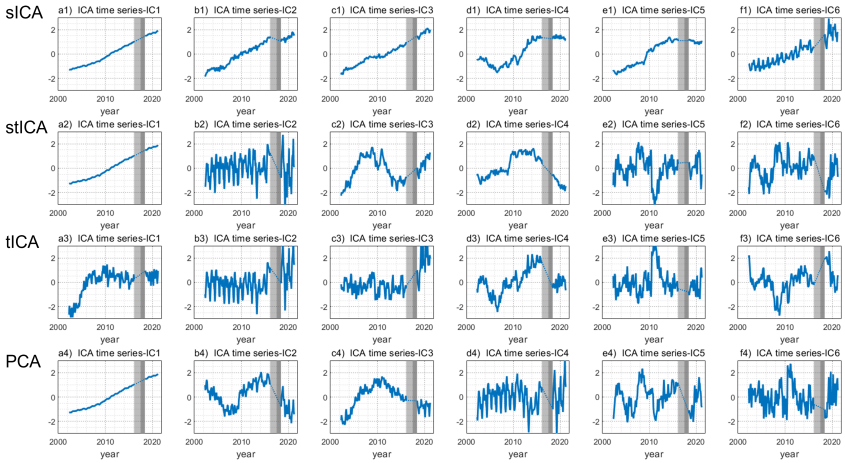

Figure 6.9: Corresponding time series of the decomposed spatial modes extracted via sICA, stICA, tICA and PCA in Fig. 6.8. The gray shading denotes the data gap in the study period, with the GRACE/GRACE-FO gap (July 2017-May 2018) in dark gray and the discarded period (July 2016-July 2017) in light gray.

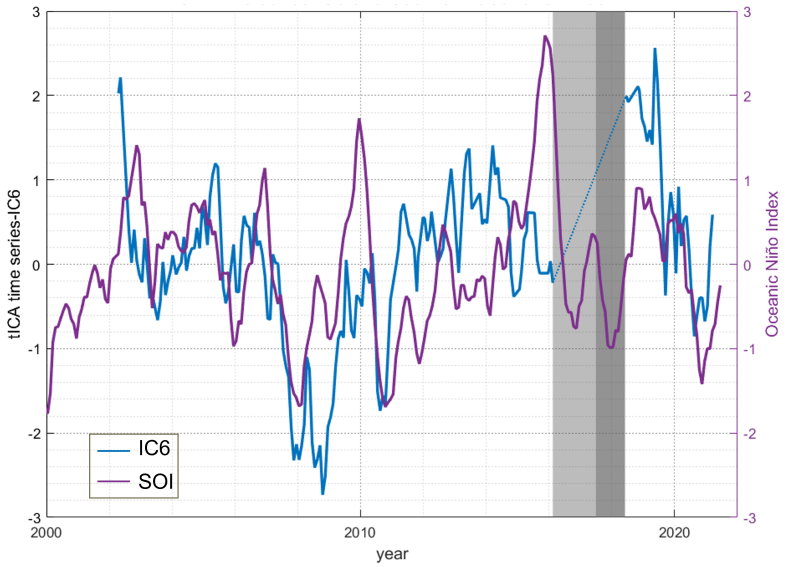

Figure 6.10: tICA time-series IC6 and Southern Oscillation Index. The gray shading denotes the data gap in the study period, with the GRACE/GRACE-FO gap (July 2017-May 2018) in dark gray and the discarded period (July 2016-July 2017) in light gray.

different scenarios; therefore, we tested three ICA methods, sICA, tICA, and stICA, and compared their results with those of the classical PCA method to determine the most appropriate method for AIS studies. The results are shown in Figs 6.8 and 6.9.

We processed the data in the same way, with the first six components selected for each of the methods. Contrast to the sICA results in the Sec.4.1.2, the six tICA spatial modes (Figs 6.8 a3-f3) are extremely similar, while the corresponding time series (Figs 6.9 a3–f3) exhibit diverse periodicities at different time scales. The tICA results may represent AIS-scale characteristics over different periods. For example, IC1 shows a dramatic shift in the trend from 2003 to 2007, IC2 and IC3 clearly reflect annual AIS variations, and IC4, IC5, and IC6 exhibit potential periodic variations at 10+-, 3–4-, and 5–6-year time scales, respectively.

We particularly found that IC6 may be correlated with the Southern Oscillation Index (SOI) (Fig. 6.10), which responds to the intensity of the possible ENSO and La Ni thicksimna activities. The overall trend and periodicity are well matched between SOI

and IC6, with the exception of some degree of divergence in 2006 and 2016, which may demonstrate the tele-coupling of the AIS with ocean activity.

The stICA results can be considered a trade-off between sICA and tICA (Figs 6.8 a2-f2 and 6.9 a2-f2). stICA can effectively extract independent features in the temporal domain, such as IC2, IC5, and IC6, which are closer to the periodic signals that were separated via tICA than those that were separated via sICA. At the same time, more spatial details can also be obtained via stICA compared with tICA, such as the separation of the spatial features of the abnormal snowfall events across East Antarctica in Mode-5.

We also compared the ICA with the classic PCA method (Figs 6.8 a4-f4 and 6.9 a4-f4). The first six principal components of PCA accounted for 58%, 5.5%, 4.7%, 3.3%, 2.2%, and 2.0% of the total variation, respectively. The first component shows the dominant long-term trend of the AIS, whose spatial Mode-1 is almost identical to the regressed linear trend (Fig. 1.1). The second component exhibits long-period variations, with East and West Antarctica in an opposite phase. The third component shows mixed signals from the Antarctic Peninsula and Wilkes Land. The fourth component shows annual variations, while the fifth and sixth components show periodic variations at medium-term time scales. The PCA results are somewhat similar to the tICA results, in that they largely represent AIS-scale characteristics, which leads to a concise and clear time series, whereas the spatial features are ambiguous and difficult to identify.

The most important difference between PCA and the three ICA methods is that PCA does not capture physical processes, such that each PCA component is a superposition of multiple physical processes. Therefore, it is impossible to extract independent physical processes of interest for a specialized study via PCA.

The GIA-related signal, which possesses the most significant uncertainty across the AIS, can only be effectively separated via sICA. We are also more familiar with some spatially distinct regions than the periodic time series, such as the intense ice melting in the AMS and the snow accumulation in East Antarctica. Identifying these spatial features will help us more easily relate the ICA results to specific physical processes. Therefore, we prefer to use ICA by maximizing the independence on the spatial domain in this study, and will also consider the combination of other ICA methods for further comparisons

with atmospheric models and reanalysis data in the future.

6.2 Stability of ICA Results

In Sec.6.1, the factors that can affect the results of ICA are discussed, including different time periods, data centers, and ICA algorithms. It is clear that the results of ICA are variable and can be influenced by many factors. But the statistical independence components in ICA results are expected to be related to physically independent processes. The variability of the ICA result will obviously weaken its credibility. This section will discuss the stability of ICA, using the analysis of GRACE/GRACE-FO as an example, to demonstrate the reliability of ICA analysis for AIS mass change.

6.2.1 Determination of Independent Component numbers

Determining the number of ICs is very important in the application of ICA. An excess number of components can make the results difficult to interpret, while insufficient components may lead to independent signals can not be effectively separated. The selection of an appropriate number of independent components requires further discussion. In this section, the number of components is adjusted to test the changes. The number of independent components will be adjusted to determine the differences in separation results for different given values and to evaluate their stability.

Here, GRACE/GRACE-FO data and sICA is used as an example, keeping the same data processing and algorithm, only the number of independent components (N) will be changed. In the previous sections, N is determined to be **6** based on the cumulative variance contribution ratio suggested by PCA (Fig. 6.5) that possesses above **70%** of the total variance. Here, the value of N is reduced from 6 to 3 by step, and the sICA separation results for each given value of N are shown in Fig. 6.11 and Fig. 6.12. Fig. 6.11 represents the spatial modes and Fig. 6.12 represents the corresponding time series of decomposed spatial modes with the same arrangement.

The first column on the left is the results for N=6, which is the rearrangement of Fig. 4.1 and Fig. 4.2 (see Sec.4.1.2). The second column is the result for N=5. Most of the components are similar to those when N=6. Mode-1, Mode-3, Mode-4, and Mode-5

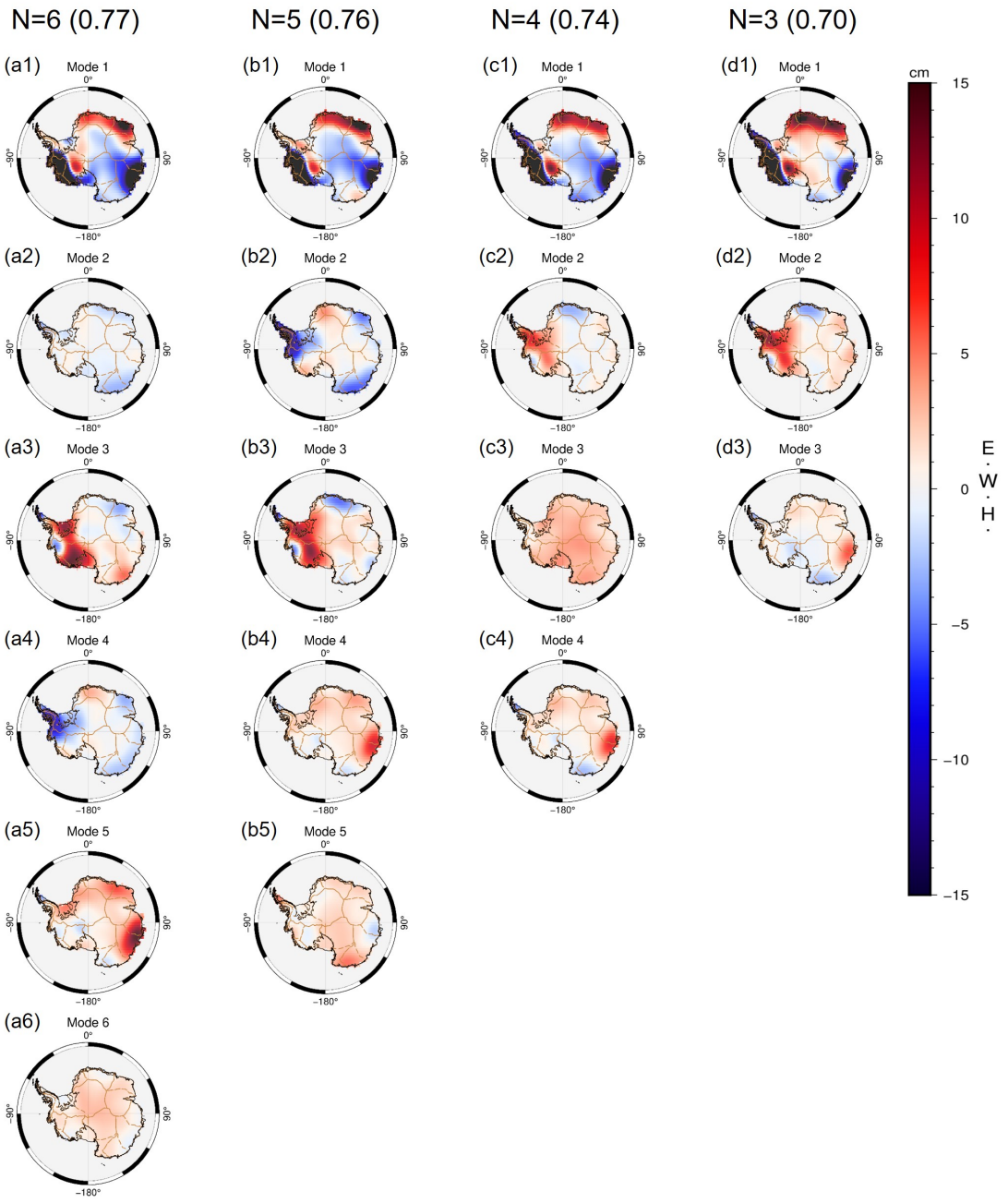

Figure 6.11: The spatial modes extracted via sICA with different independent component numbers (N). From left to right, each column is the separated spatial modes when N is 6,5,4,3, respectively

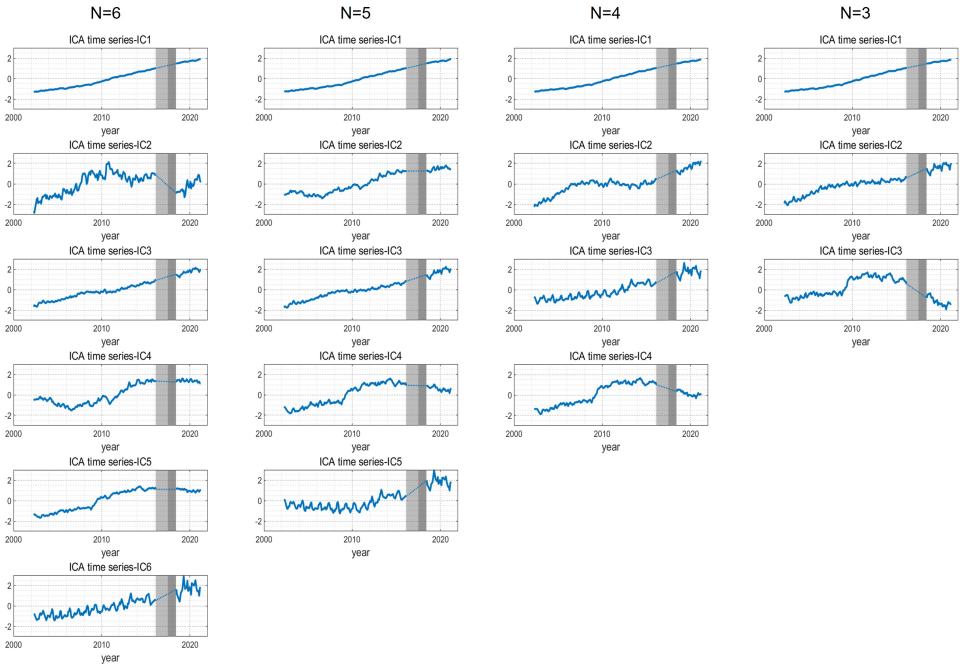

Figure 6.12: Corresponding time series of the decomposed spatial modes extracted via sICA with different independent component numbers (N) in Fig. 6.11. From left to right, each column is the spatial mode when N is 6,5,4,3, respectively. The gray shading denotes the data gap in the study period, with the GRACE/GRACE-FO gap (July 2017-May 2018) in dark gray and the discarded period (July 2016-July 2017) in light gray.

can be found to be completely consistent in the results of N=6. Specifically, (b1)–(a1), (b3)–(a3), (b4)–(a5) and (b5)–(a6) can be paired with each other. It is worth noting that (b2) appears as a combination of (a2) and (a4).

The situation is similar when N=4. (c1)–(b1), (c2)–(b3), (c3)–(b5) and (c4)–(b4) can be considered as corresponding pairs. It is very interesting to note that (b1) and (b2) could be further combined into one component (c1). It can be confirmed by comparing the spatial distribution of (c1) in Fig. 6.11 with (b1) and (c1). The mass loss signal especially in the north tip of AP and GVL areas suggested by (b2) that is not included in (b1) can be found in (c1).

As $\boldsymbol{N}$ is further reduced to 3, (d1)–(c1), (d2)–(c2), and (d3)–(c4) can be considered as corresponding pairs. The periodic mass increase of overall AIS suggested by (c3) cannot be found when N=3. (c1) and (c3) could be further combined into one component (d1). Compared to (c1), the spatial distribution of (d1) in Fig. 6.11 does not show a clear trend of mass loss over the inland area of Antarctica which could be due to the superposition of (c1) and (c3).

Overall, the decomposition results of sICA with different IC numbers show very good stability. No conflicting results are obtained. Components that are associated with glacier/snow changes ((a1), (b1), (c1) and (d1)), extreme snowfall events ((a5), (b4), (c4) and (d3)) and GIA ((a3), (b3), (c2) and (d2)) can be found in all situations. It can be concluded that as $\boldsymbol{N}$ decreases, the decomposition becomes more incomplete and the integration of signals becomes more significant.

Furthermore, decreasing N reveals the processes signal mixing, and their order implies the strength of independence of each component. From the results of N=3, it can be found that glacier/snow change, GIA, and extreme snowfall events may have the strongest independence. In phase $\boldsymbol{N = 4 \sim 3}$, a periodic variation with annual cycle can be separated from the glacier/snow changes, and this annual signal has relatively strong independence. In phase $\boldsymbol{N = 5 \sim 4}$, glacier changes in the AP and GVL areas can be separated from the remaining glaciers like AMS, implying the different dominant physical processes for these areas. The time series of (b2) in Fig. 6.12 exhibits a more complex periodicity when compared with (b1). In phase $\boldsymbol{N = 6 \sim 5}$, it can be found that AP

exhibits a different multi-year periodic pattern with regions such as GVL that could be controlled by different climate factors.

This inverse process also shows how the independent components are decomposed and effectively helps to understand the signal mixing process in Antarctica and the relationships between different components.

6.2.2 Representation of Spatial Field

Commonly, the time-varying gravity field can be represented by the geoid $\boldsymbol{N}$. The geoid height can be calculated using a series of fully normalized SH Coefficients provided by GRACE level-2 products as follows Wahr et al. (1998):

$$\boldsymbol{N(\theta,\lambda) = a\sum_{l=0}^{\infty}\sum_{m=0}^{l}\overline{P_{lm}}(cos\theta)[C_{lm}cos(m\lambda) + S_{lm}sin(m\lambda)]} \tag{6.1}$$

Where $\boldsymbol{a}$ is the average radius of the Earth, $\boldsymbol{\theta}$ and $\boldsymbol{\lambda}$ represent latitude and longitude, $\boldsymbol{\overline{P_{lm}}(cos\theta)}$ is the normalized associated Legendre function, $\boldsymbol{C_{lm}}$ and $\boldsymbol{S_{lm}}$ are the fully normalized SH coefficients of the Earth's gravity field, $\boldsymbol{l}$ and $\boldsymbol{m}$ are the degree and order of SH coefficients respectively.

The mass transfer and redistribution on the Earth's surface will cause the change of geoid. This change can be expressed by the changes of SH coefficients $\boldsymbol{\Delta\overline{C_{lm}}}$ and $\boldsymbol{\overline{\Delta S_{lm}}}$:

$$\boldsymbol{\Delta N\,(\theta,\lambda) = a\sum_{l=0}^{\infty}\sum_{m=0}^{l}\overline{P_{lm}}\,(cos\theta)\,\left(\Delta\overline{C_{lm}}cos(m\lambda) + \Delta\overline{S_{lm}}sin(m\lambda)\right)} \tag{6.2}$$

Where $\boldsymbol{\Delta\overline{C_{lm}}}$, $\boldsymbol{\overline{\Delta S_{lm}}}$ can be expressed as follows (Chao and Gross, 1987):

$$\boldsymbol{\begin{Bmatrix}\Delta\overline{C_{lm}}\\ \Delta\overline{S_{lm}}\end{Bmatrix} = \frac{3}{4\pi a\rho_E\,(2l+1)}\int\Delta\rho(r,\theta,\lambda)\overline{P_{lm}}(cos\theta)(\frac{r}{a})^{l+2}\begin{Bmatrix}cos(m\lambda)\\ sin(m\lambda)\end{Bmatrix}sin\theta d\theta d\lambda dr} \tag{6.3}$$

$\boldsymbol{\rho_E}$ represents the average density of the Earth.

SH is completely defined basis on the sphere, it allows for the representation of functions on the surface of a sphere with high accuracy. The series expansion of a function in spherical harmonics is often more computationally efficient. This makes it particularly useful for large-scale problems.

Generally, the SH coefficients published by the data center need to be transformed into spatial field before ICA. Therefore, the input data for ICA is in the form of spatial grid. All the previous results obtained above are calculated in this way. The alternative way is to directly analyze with SH coefficients, which will generate the results in SH expansion, and then to inverse the results to a spatial field. Although there are two different ways (as shown in Fig. 6.13), they are expected to be completely equivalent because the input data contains exactly the same information only differ in the representation formation.
Here, GRACE/GRACE-FO data will be used as an example, keeping the same data processing and algorithm to compare the results through the two ways. The comparison of the two ways are shown in Fig. 6.14. The sICA results based on the SH expansion and the spatial grid input are presented on the left and right sides, respectively. For ease of comparison, the right panel presents a reorganized version of Fig. 4.1 and Fig. 4.2.
The results of ICA analysis based on SH expansion and grid are highly comparable in some of their time series, among them IC4, IC5 and IC6 can be considered equivalent. However, noticeable differences can also be observed in the spatial distribution, particularly in Mode-1, Mode-2, and Mode-3. For SH-based results, Mode-1 exhibits a long-term mass decrease in WA, while EA shows a spatially simple long-term mass increase. Different from grid-based results, the areas like Totten do not have mass decrease trend, in contrast, Mode-3 exhibits the mass decrease trend in DML and Totten, as well as AMS in WA, which suggests that the results of the analysis with SH-based input can not distinguish the two linear components very well. Mode-2 is mainly differs in AP, SH-based Mode-2 does not separate the AP from the rest of the region as another independent component which approximates to the grid-based decomposition with independent component of N=5 ((b2) in Fig. 6.11 and Fig. 6.12).
Furthermore, discrepancies are noticeable in the ocean region. Stripe-like signals persist in the SH results due to the application of the ocean/land mask. Since the focus of this study is solely on terrestrial mass changes, a mask is employed to eliminate signals originating from the ocean. However, the truncation of SH expansion induces signal leakage at the ocean/land boundary.
Similar comparisons were also performed using stICA and tICA, the results of which are

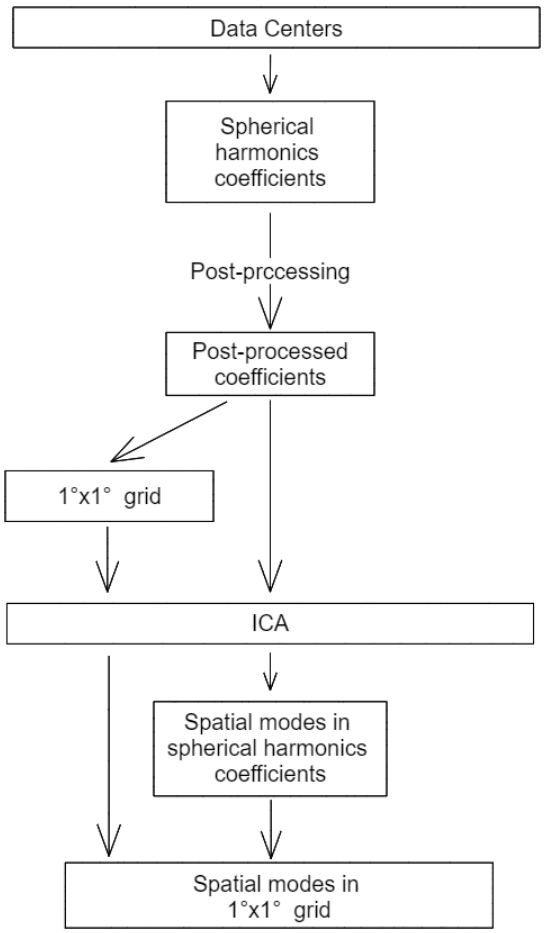

Figure 6.13: Two different ICA input data processing flows.

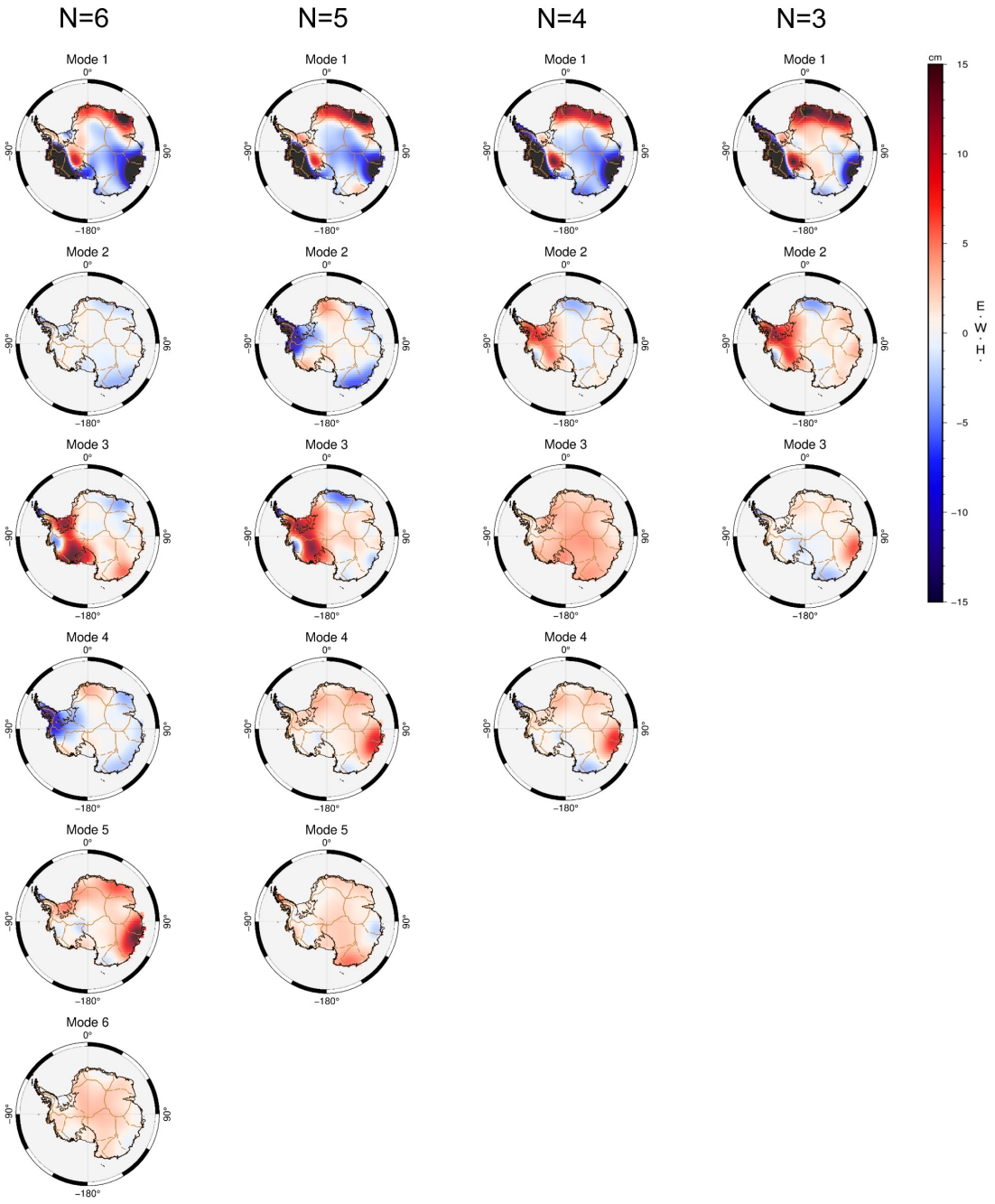

Figure 6.14: Comparison of sICA results of GRACE/GRACE-FO with different representation formation. The left and right are the input represented by SH and spatial gird, respectively.

presented in Fig. 6.15 and Fig. 6.16. In comparison to sICA, these two algorithms are focused more on the temporal independence, thus the differences caused by the expression of spatial data should be weaker. It can be seen that apart from a change in the ordering of the components, the ICA results from SH and Grid are almost identical.
Similar comparisons are also been repeated using stICA and tICA. The results are shown in Fig. 6.15 and Fig. 6.16, respectively. Compared to sICA, these two algorithms more focus on independence in temporal domain, thus the differences caused by the expression of spatial data should be even more subtle. It can be seen that apart from a change in the ordering of the components, the ICA results from SH and Grid are almost identical. Therefore, it can be concluded that, theoretically, the organization format of data will not affect the results of ICA as long as the data contains the same information. However, the use of Ocean/Land mask will leads to significant errors in the spatial domain due to truncation errors, which can severely interfere with the results. Overall, the performance of the decomposition using spatial grid as input is superior to that using SH expansion as input.

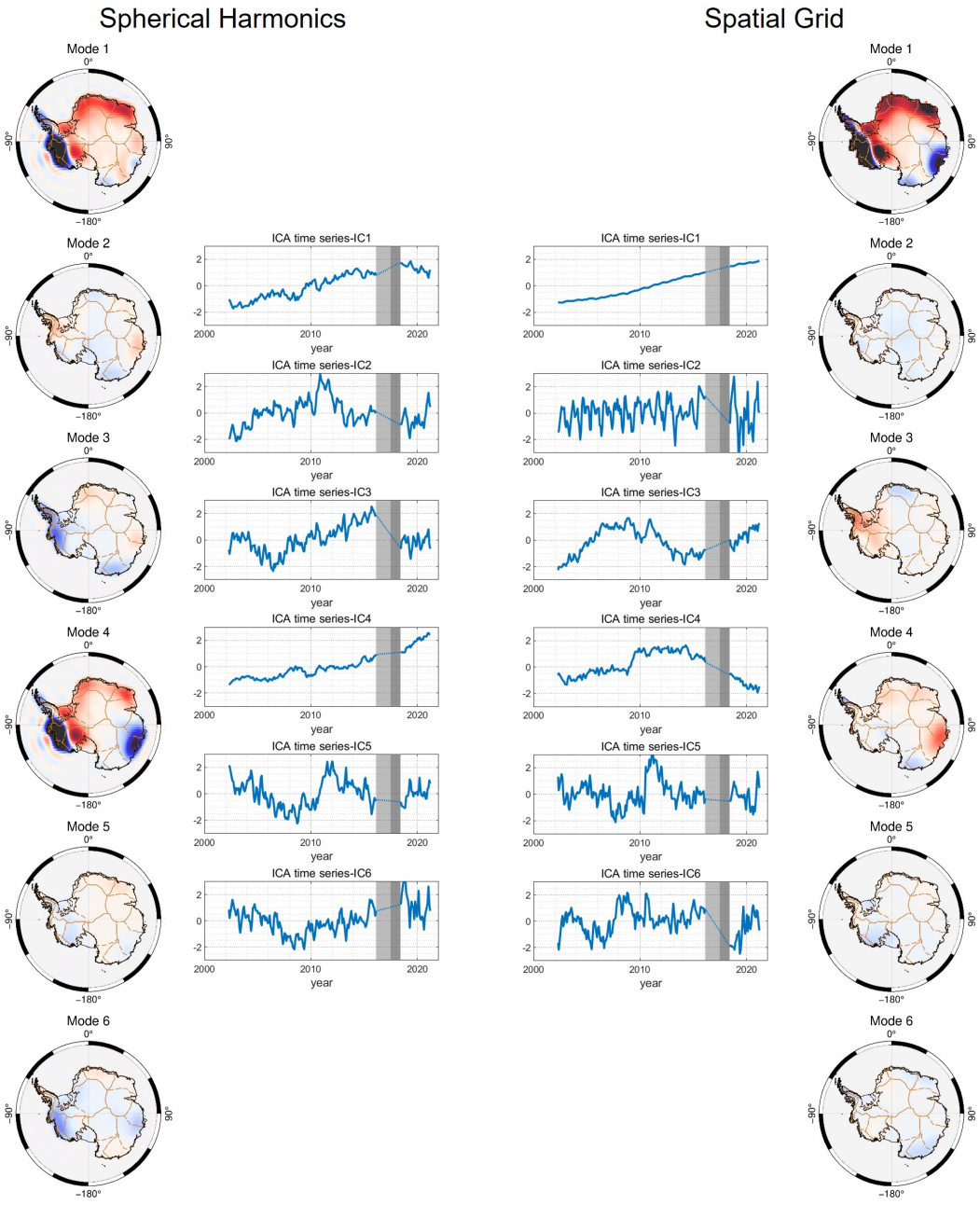

Figure 6.15: Comparison of stICA results of GRACE/GRACE-FO with different representation formation. The left and right are the input represented by SH and spatial gird, respectively.

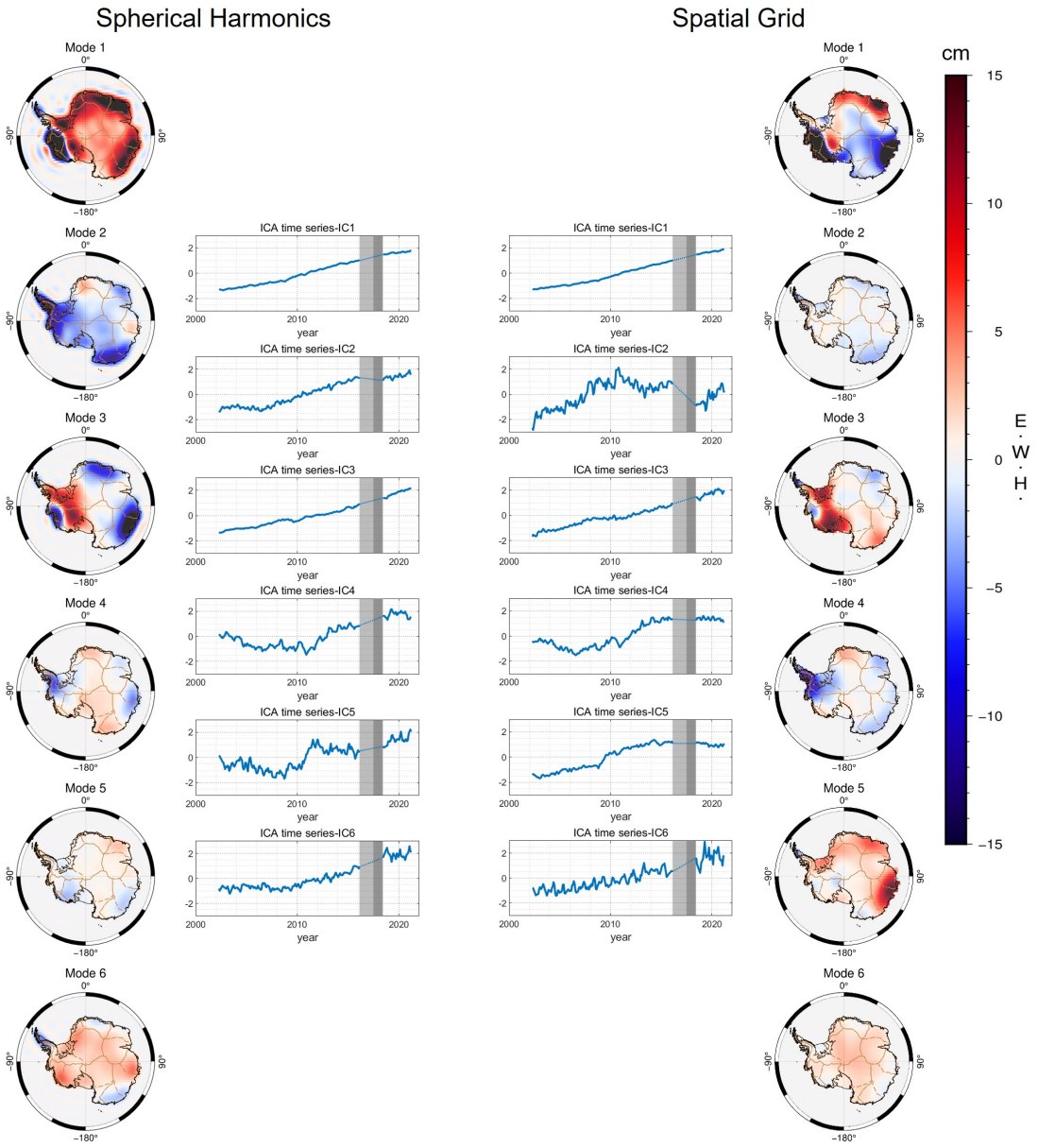

Figure 6.16: Comparison of tICA results of GRACE/GRACE-FO with different representation formation. The left and right are the input represented by SH and spatial gird, respectively.

Chapter 7

Conclusion and Future Work

7.1 Conclusion

This dissertation revisited the main physical processes of AIS from a satellite geodetic perspective. When reviewing the available data just realized that we have a decades-long record of observations for the AIS study. This dissertation focused on the utilization of statistical information of satellite data, using ICA method as a framework to achieve a different perspective to analyze the changes in AIS. The main conclusions obtained are as follows:

1. The spatio-temporal properties of AIS variations were extracted using ICA. Typical long-term trends (e.g., mass loss in WA) were clearly extracted and linked to physical processes that can be easily recognized, such as glacier and snowfall such as ice dynamics, snowfall and GIA. For time series with complex periodic signals, such as those observed in AP, which are presumed to originate from the ocean current, further investigation is required.

2. The results of GRACE/GRACE-FO are corroborated with the altimeter data. For comparison purposes, suitable approaches of unifying resolutions were discussed. Notable common signals in both gravity field and elevation changes like snow/ice trend, snowfall were confirmed by mutual comparison. Which proved that the ICA results are reliable and directed to trustworthy physical processes.

3. The separation results were examined using physical models. GIA signal from

GRACE/GRACE-FO observations has been achieved for the first time. This is further confirmed by four forward GIA models. However, due to the limitations of the ICA method, this study did not effectively constrain the GIA modeling and quantitatively evaluate the GIA model based on the separation results.

4. An Antarctica SMB model (NHM) was introduced to study AIS drainage basins. A Classification of basins was proposed based on the behaviors of total mass changes, SMB mass changes and surface elevation changes. Dominant physical processes in each region could be identified by combining the results of the ICA analysis and SMB model.

5. The robustness of ICA results was also examined. Some of the factors affecting ICA results were discussed and summarized. The time period of the input data was found to have a direct effect on the results. By adjusting the number of independent components, it has been demonstrated that the glacier changes, snowfall pattern, and GIA pattern separated exhibit strong stability. This demonstrated the clear association of the ICA results and specific physical processes. In addition, regarding the ICA algorithm, it is concluded that for most geophysical signals using sICA to separate independent sub-regions is more straightforward and comprehensible.

7.2 Future work

Investigating of periodic components

Further work is also needed to focus more on the periodic components, since these components are much possible to connect with meteorological factors that are globally correlated. This helps understand the response of AIS to current–near future global climate change as well as possible teleconnection.

Constraining ice history for GIA modeling

The GIA signal separated using ICA is hard to be quantified, while its spatial distribution is demonstrated to be stable. The viscoelastic parameters of the Earth is less sensitive to spatial distribution compared to that of ice history. Therefore,

it is worth considering the use of ICA results to constrain the ice history in future studies.

Involving the ocean effect

The ocean is an important driver affecting AIS, but the role of the ocean is not considered much in this stage because of the lack of relevant knowledge. The influence of the ocean needs to be incorporated in the future.

Limited spatial resolution

Gravity satellite-GRACE has a natural advantage for studying mass changes but is limited by its spatial resolution (about 300km). Higher spatial resolution is important for understanding processes such as frequently occurring coastal sea-ice interactions and mass redistribution within glacier basins. Several studies indicate the possibility of further enhancing its resolution in Antarctica, such as using mascon solution. This needs to be further considered in the future.

Bibliography

Cécile Agosta, Charles Amory, Christoph Kittel, Anais Orsi, Vincent Favier, Hubert Gallée, Michiel R. van den Broeke, Jan T. M. Lenaerts, Jan Melchior van Wessem, Willem Jan van de Berg, and Xavier Fettweis. Estimation of the Antarctic surface mass balance using the regional climate model MAR (1979–2015) and identification of dominant processes. *The Cryosphere*, 13(1):281–296, January 2019. ISSN 1994-0424. doi: 10.5194/tc-13-281-2019. 2.1.1, 2.1.2

R.O. Anyah, E. Forootan, J.L. Awange, and M. Khaki. Understanding linkages between global climate indices and terrestrial water storage changes over Africa using GRACE products. *Science of The Total Environment*, 635:1405–1416, September 2018. ISSN 00489697. doi: 10.1016/j.scitotenv.2018.04.159. 3.2

J.L. Awange, E. Forootan, M. Kuhn, J. Kusche, and B. Heck. Water storage changes and climate variability within the Nile Basin between 2002 and 2011. *Advances in Water Resources*, 73:1–15, November 2014. ISSN 03091708. doi: 10.1016/j.advwatres.2014.06.010. 3.2

Chandan Banerjee and D. Nagesh Kumar. Analyzing Large-Scale Hydrologic Processes Using GRACE and Hydrometeorological Datasets. *Water Resources Management*, 32 (13):4409–4423, October 2018. ISSN 1573-1650. doi: 10.1007/s11269-018-2070-x. 3.2

Anthony J. Bell and Terrence J. Sejnowski. An Information-Maximization Approach to Blind Separation and Blind Deconvolution. *Neural Computation*, 7(6):1129–1159, November 1995. ISSN 0899-7667. doi: 10.1162/neco.1995.7.6.1129. 3.1.2

Carmen Boening, Matthew Lebsock, Felix Landerer, and Graeme Stephens. Snowfall-driven mass change on the East Antarctic ice sheet. *Geophysical Research Letters*, 39 (21), 2012. ISSN 1944-8007. doi: 10.1029/2012GL053316. 4.1.2, 5.2.1

Eva Boergens, Elena Rangelova, Michael G. Sideris, and Juergen Kusche. Assessment of the capabilities of the temporal and spatiotemporal ICA method for geophysical signal separation in GRACE data. *Journal of Geophysical Research: Solid Earth*, 119 (5):4429–4447, May 2014. ISSN 21699313. doi: 10.1002/2013JB010452. 5.1

J. Cardoso. Infomax and maximum likelihood for blind source separation. *IEEE Signal Processing Letters*, 4(4):112–114, April 1997. ISSN 1070-9908. doi: 10.1109/97.566704. 3.1.2

J.-F. Cardoso. Fourth-order cumulant structure forcing: Application to blind array processing. In *[1992] IEEE Sixth SP Workshop on Statistical Signal and Array Processing*, pages 136–139, Victoria, BC, Canada, 1992. IEEE. ISBN 978-0-7803-0508-3. doi: 10.1109/SSAP.1992.246830. 3.2

B. Fong Chao and Richard S. Gross. Changes in the Earth's rotation and low-degree gravitational field induced by earthquakes. *Geophysical Journal of the Royal Astronomical Society*, 91(3):569–596, 1987. ISSN 1365-246X. doi: 10.1111/j.1365-246X.1987.tb01659.x. 6.2.2

J. L. Chen. Satellite Gravity Measurements Confirm Accelerated Melting of Greenland Ice Sheet. *Science*, 313(5795):1958–1960, September 2006. ISSN 0036-8075, 1095-9203. doi: 10.1126/science.1129007. 2.2.1

Pierre Comon. Independent Component Analysis, a new concept? *Signal Processing*, 36: 287–314, April 1994. doi: 10.1016/0165-1684(94)90029-9. 3.1.2

E. Forootan and J. Kusche. Separation of global time-variable gravity signals into maximally independent components. *Journal of Geodesy*, 86(7):477–497, July 2012. ISSN 0949-7714, 1432-1394. doi: 10.1007/s00190-011-0532-5. 3.1.2, 3.2

P. Fretwell, H. D. Pritchard, D. G. Vaughan, J. L. Bamber, N. E. Barrand, R. Bell, C. Bianchi, R. G. Bingham, D. D. Blankenship, G. Casassa, G. Catania, D. Callens, H. Conway, A. J. Cook, H. F. J. Corr, D. Damaske, V. Damm, F. Ferraccioli, R. Forsberg, S. Fujita, Y. Gim, P. Gogineni, J. A. Griggs, R. C. A. Hindmarsh, P. Holmlund, J. W. Holt, R. W. Jacobel, A. Jenkins, W. Jokat, T. Jordan, E. C. King, J. Kohler, W. Krabill, M. Riger-Kusk, K. A. Langley, G. Leitchenkov, C. Leuschen, B. P. Luyendyk, K. Matsuoka, J. Mouginot, F. O. Nitsche, Y. Nogi, O. A. Nost, S. V. Popov, E. Rignot, D. M. Rippin, A. Rivera, J. Roberts, N. Ross, M. J. Siegert, A. M. Smith, D. Steinhage, M. Studinger, B. Sun, B. K. Tinto, B. C. Welch, D. Wilson, D. A. Young, C. Xiangbin, and A. Zirizzotti. Bedmap2: Improved ice bed, surface and thickness datasets for Antarctica. *The Cryosphere*, 7(1):375–393, February 2013. ISSN 1994-0424. doi: 10.5194/tc-7-375-2013. (document), 4.1.2, 5.5, 5.2.1

A Geruo, John Wahr, and Shijie Zhong. Computations of the viscoelastic response of a 3-D compressible Earth to surface loading: An application to Glacial Isostatic Adjustment in Antarctica and Canada. *Geophysical Journal International*, 192(2): 557–572, February 2013. ISSN 0956-540X, 1365-246X. doi: 10.1093/gji/ggs030. 5.1

A. Hattori, Y. Aoyama, J. Okuno, and K. Doi. GNSS observations of GIA-induced crustal deformation in Lützow-Holm Bay, East Antarctica. *Geophysical Research Letters*, June 2021. ISSN 0094-8276, 1944-8007. doi: 10.1029/2021GL093479. 2.1.3

Daisuke Hirano, Takeshi Tamura, Kazuya Kusahara, Kay I. Ohshima, Keith W. Nicholls, Shuki Ushio, Daisuke Simizu, Kazuya Ono, Masakazu Fujii, Yoshifumi Nogi, and Shigeru Aoki. Strong ice-ocean interaction beneath Shirase Glacier Tongue in East Antarctica. *Nature Communications*, 11(1):4221, December 2020. ISSN 2041-1723. doi: 10.1038/s41467-020-17527-4. 2.1.1

Daisuke Hirano, Kohei Mizobata, Hiroko Sasaki, Hiroto Murase, Takeshi Tamura, and Shigeru Aoki. Poleward eddy-induced warm water transport across a shelf break off Totten Ice Shelf, East Antarctica. *Communications Earth & Environment*, 2(1):153, December 2021. ISSN 2662-4435. doi: 10.1038/s43247-021-00217-4. 4.1.2

Erik R. Ivins and Thomas S. James. Antarctic glacial isostatic adjustment: a new assessment. *Antarctic Science*, 17(4):541–553, December 2005. ISSN 0954-1020, 1365-2079. doi: 10.1017/S0954102005002968. URL https://www.cambridge.org/core/product/identifier/S0954102005002968/type/journal_article. 2.2.1

Erik R. Ivins, Thomas S. James, John Wahr, Ernst J. O. Schrama, Felix W. Landerer, and Karen M. Simon. Antarctic contribution to sea level rise observed by GRACE with improved GIA correction: ANTARCTIC GIA AND RECENT ICE MASS LOSS. *Journal of Geophysical Research: Solid Earth*, 118(6):3126–3141, June 2013. ISSN 21699313. doi: 10.1002/jgrb.50208. 5.1

Byeong-Hoon Kim, Ki-Weon Seo, Jooyoung Eom, Jianli Chen, and Clark R. Wilson. Antarctic ice mass variations from 1979 to 2017 driven by anomalous precipitation accumulation. *Scientific Reports*, 10(1):20366, December 2020. ISSN 2045-2322. doi: 10.1038/s41598-020-77403-5. 4.2.2

Matt A. King, Rory J. Bingham, Phil Moore, Pippa L. Whitehouse, Michael J. Bentley, and Glenn A. Milne. Lower satellite-gravimetry estimates of Antarctic sea-level contribution. *Nature*, 491(7425):586–589, November 2012. ISSN 1476-4687. doi: 10.1038/nature11621. 2.2.1

J. Kusche, R. Schmidt, S. Petrovic, and R. Rietbroek. Decorrelated GRACE time-variable gravity solutions by GFZ, and their validation using a hydrological model. *Journal of Geodesy*, 83(10):903–913, October 2009. ISSN 1432-1394. doi: 10.1007/s00190-009-0308-3. 4.1.1

Glen E. Liston, Jan-Gunnar Winther, Oddbjørn Bruland, Hallgeir Elvehøy, and Knut Sand. Below-surface ice melt on the coastal Antarctic ice sheet. *Journal of Glaciology*, 45(150):273–285, 1999. ISSN 0022-1430, 1727-5652. doi: 10.3189/S0022143000001775. 2.1.1

Bryant D. Loomis, Kenneth E. Rachlin, David N. Wiese, Felix W. Landerer, and Scott B. Luthcke. Replacing GRACE/GRACE-FO With Satellite Laser Ranging: Impacts on

Antarctic Ice Sheet Mass Change. *Geophysical Research Letters*, 47(3), February 2020. ISSN 0094-8276, 1944-8007. doi: 10.1029/2019GL085488. 4.1.1

Scott B. Luthcke, T. J. Sabaka, B. D. Loomis, A. A. Arendt, J. J. McCarthy, and J. Camp. Antarctica, Greenland and Gulf of Alaska land-ice evolution from an iterated GRACE global mascon solution. *Journal of Glaciology*, 59(216):613–631, 2013/ed. ISSN 0022-1430, 1727-5652. doi: 10.3189/2013JoG12J147. 2.2.1

Robert A. Massom and Sharon E. Stammerjohn. Antarctic sea ice change and variability – Physical and ecological implications. *Polar Science*, 4(2):149–186, August 2010. ISSN 1873-9652. doi: 10.1016/j.polar.2010.05.001. 1

Mathieu Morlighem, Eric Rignot, Tobias Binder, Donald Blankenship, Reinhard Drews, Graeme Eagles, Olaf Eisen, Fausto Ferraccioli, René Forsberg, Peter Fretwell, Vikram Goel, Jamin S. Greenbaum, Hilmar Gudmundsson, Jingxue Guo, Veit Helm, Coen Hofstede, Ian Howat, Angelika Humbert, Wilfried Jokat, Nanna B. Karlsson, Won Sang Lee, Kenichi Matsuoka, Romain Millan, Jeremie Mouginot, John Paden, Frank Pattyn, Jason Roberts, Sebastian Rosier, Antonia Ruppel, Helene Seroussi, Emma C. Smith, Daniel Steinhage, Bo Sun, Michiel R. van den Broeke, Tas D. van Ommen, Melchior van Wessem, and Duncan A. Young. Deep glacial troughs and stabilizing ridges unveiled beneath the margins of the Antarctic ice sheet. *Nature Geoscience*, 13(2):132–137, February 2020. ISSN 1752-0908. doi: 10.1038/s41561-019-0510-8. 4.1.2

W. Richard Peltier, Donald F. Argus, and Rosemarie Drummond. Comment on "An Assessment of the ICE-6G_C (VM5a) Glacial Isostatic Adjustment Model" by Purcell et al. *Journal of Geophysical Research: Solid Earth*, 123(2):2019–2028, 2018. ISSN 2169-9356. doi: 10.1002/2016JB013844. 5.1

H. D. Pritchard, S. R. M. Ligtenberg, H. A. Fricker, D. G. Vaughan, M. R. van den Broeke, and L. Padman. Antarctic ice-sheet loss driven by basal melting of ice shelves. *Nature*, 484(7395):502–505, April 2012. ISSN 1476-4687. doi: 10.1038/nature10968. 2.1.1

Michael B. Richman. Rotation of principal components. *Journal of Climatology*, 6(3): 293–335, 1986. ISSN 1097-0088. doi: 10.1002/joc.3370060305. 3.1.1

E. Rignot, S. Jacobs, J. Mouginot, and B. Scheuchl. Ice-Shelf Melting Around Antarctica. *Science*, 341(6143):266–270, July 2013. ISSN 0036-8075, 1095-9203. doi: 10.1126/science.1235798. (document), 5.2, 5.2, 5.3

Eric Rignot, Jérémie Mouginot, Bernd Scheuchl, Michiel van den Broeke, Melchior J. van Wessem, and Mathieu Morlighem. Four decades of Antarctic Ice Sheet mass balance from 1979–2017. *Proceedings of the National Academy of Sciences*, 116(4):1095–1103, January 2019. ISSN 0027-8424, 1091-6490. doi: 10.1073/pnas.1812883116. 1

R. Riva, B. C. Gunter, T. J. Urban, B. L. A. Vermeersen, R. C. Lindenbergh, M. M. Helsen, J. L. Bamber, RSW de Wal, M. van den Broeke, and B. E. Schutz. Glacial Isostatic Adjustment over Antarctica from combined ICESat and GRACE satellite data. *Earth and Planetary Science Letters*, 288:516–523, 2009. doi: 10.1016/j.epsl.2009.10.013. 2.1.3

Martin Schmeer, Michael Schmidt, Wolfgang Bosch, and Florian Seitz. Separation of mass signals within GRACE monthly gravity field models by means of empirical orthogonal functions. *Journal of Geodynamics*, 59–60:124–132, September 2012. ISSN 0264-3707. doi: 10.1016/j.jog.2012.03.001. 3.2

R. Schmidt, F. Flechtner, U. Meyer, K.-H. Neumayer, Ch. Dahle, R. König, and J. Kusche. Hydrological Signals Observed by the GRACE Satellites. *Surveys in Geophysics*, 29(4):319–334, October 2008. ISSN 1573-0956. doi: 10.1007/s10712-008-9033-3. 3.2

Ludwig Schröder, Martin Horwath, Reinhard Dietrich, Veit Helm, Michiel R. van den Broeke, and Stefan R. M. Ligtenberg. Four decades of Antarctic surface elevation changes from multi-mission satellite altimetry. *The Cryosphere*, 13(2):427–449, February 2019. ISSN 1994-0424. doi: 10.5194/tc-13-427-2019. (document), 2.3, 4.1.2, 4.2, 5.2.1

Mehdi S. Shafiei Joud, Lars Erik Sjöberg, and Mohammad Bagherbandi. Post-Glacial Land Uplift Rate in Fennoscandia and Laurentia Determined by GRACE Data. Preprint, EARTH SCIENCES, January 2019. 3.2

A. Shepherd, E. R. Ivins, A Geruo, V. R. Barletta, M. J. Bentley, S. Bettadpur, K. H. Briggs, D. H. Bromwich, R. Forsberg, N. Galin, M. Horwath, S. Jacobs, I. Joughin, M. A. King, J. T. M. Lenaerts, J. Li, S. R. M. Ligtenberg, A. Luckman, S. B. Luthcke, M. McMillan, R. Meister, G. Milne, J. Mouginot, A. Muir, J. P. Nicolas, J. Paden, A. J. Payne, H. Pritchard, E. Rignot, H. Rott, L. S. Sorensen, T. A. Scambos, B. Scheuchl, E. J. O. Schrama, B. Smith, A. V. Sundal, J. H. van Angelen, W. J. van de Berg, M. R. van den Broeke, D. G. Vaughan, I. Velicogna, J. Wahr, P. L. Whitehouse, D. J. Wingham, D. Yi, D. Young, and H. J. Zwally. A Reconciled Estimate of Ice-Sheet Mass Balance. *Science*, 338(6111):1183–1189, November 2012. ISSN 0036-8075, 1095-9203. doi: 10.1126/science.1228102. 1

Andrew Shepherd, Lin Gilbert, Alan S. Muir, Hannes Konrad, Malcolm McMillan, Thomas Slater, Kate H. Briggs, Aud V. Sundal, Anna E. Hogg, and Marcus E. Engdahl. Trends in Antarctic Ice Sheet Elevation and Mass. *Geophysical Research Letters*, 46(14):8174–8183, 2019. ISSN 1944-8007. doi: 10.1029/2019GL082182. 2.2.2

Tianyan Shi, Yoichi Fukuda, Koichiro Doi, and Jun'ichi Okuno. Extraction of GRACE/GRACE-FO observed mass change patterns across Antarctica via independent component analysis (ICA). *Geophysical Journal International*, 229(3):1914–1926, February 2022. ISSN 0956-540X, 1365-246X. doi: 10.1093/gji/ggac033. 3.2

JV Stone and J Porrill. Regularisation Using Spatiotemporal Independence and Predictability. page 7, June 1999. 3.1.2

Matthieu J. Talpe, R. Steven Nerem, Ehsan Forootan, Michael Schmidt, Frank G. Lemoine, Ellyn M. Enderlin, and Felix W. Landerer. Ice mass change in Greenland and Antarctica between 1993 and 2013 from satellite gravity measurements. *Journal of Geodesy*, 91(11):1283–1298, November 2017. ISSN 0949-7714, 1432-1394. doi: 10.1007/s00190-017-1025-y. 3.2

The IMBIE team. Mass balance of the Antarctic Ice Sheet from 1992 to 2017. *Nature*, 558(7709):219–222, June 2018. ISSN 0028-0836, 1476-4687. doi: 10.1038/s41586-018-0179-y. 1

Michiel van den Broeke, Jonathan Bamber, Janneke Ettema, Eric Rignot, Ernst Schrama, Willem Jan van de Berg, Erik van Meijgaard, Isabella Velicogna, and Bert Wouters. Partitioning Recent Greenland Mass Loss. *Science*, 326(5955):984–986, November 2009. ISSN 0036-8075, 1095-9203. doi: 10.1126/science.1178176. 1

Michiel R. Van Den Broeke, Carleen H. Reijmer, and Roderik S.W. Van De Wal. A study of the surface mass balance in Dronning Maud Land, Antarctica, using automatic weather stationS. *Journal of Glaciology*, 50(171):565–582, 2004. ISSN 0022-1430, 1727-5652. doi: 10.3189/172756504781829756. 2.1.1

Jan Melchior van Wessem, Willem Jan van de Berg, Brice P. Y. Noël, Erik van Meijgaard, Charles Amory, Gerit Birnbaum, Constantijn L. Jakobs, Konstantin Krüger, Jan T. M. Lenaerts, Stef Lhermitte, Stefan R. M. Ligtenberg, Brooke Medley, Carleen H. Reijmer, Kristof van Tricht, Luke D. Trusel, Lambertus H. van Ulft, Bert Wouters, Jan Wuite, and Michiel R. van den Broeke. Modelling the climate and surface mass balance of polar ice sheets using RACMO2 – Part 2: Antarctica (1979–2016). *The Cryosphere*, 12(4):1479–1498, April 2018. ISSN 1994-0416. doi: 10.5194/tc-12-1479-2018. 2.1.2, 2.2.1

I. Velicogna and J. Wahr. Time-variable gravity observations of ice sheet mass balance: Precision and limitations of the GRACE satellite data. *Geophysical Research Letters*, 40(12):3055–3063, 2013. ISSN 1944-8007. doi: 10.1002/grl.50527. 1

Isabella Velicogna and John Wahr. Measurements of Time-Variable Gravity Show Mass Loss in Antarctica. *Science*, 311(5768):1754–1756, March 2006. ISSN 0036-8075, 1095-9203. doi: 10.1126/science.1123785. 2.2.1

Isabella Velicogna, Yara Mohajerani, Geruo, Felix Landerer, Jeremie Mouginot, Brice Noel, Eric Rignot, Tyler Sutterley, Michiel van den Broeke, Melchior van Wessem, and

David Wiese. Continuity of Ice Sheet Mass Loss in Greenland and Antarctica From the GRACE and GRACE Follow-On Missions. *Geophysical Research Letters*, 47(8): e2020GL087291, 2020. ISSN 1944-8007. doi: 10.1029/2020GL087291. 4.1.1

John Wahr, Mery Molenaar, and Frank Bryan. Time variability of the Earth's gravity field: Hydrological and oceanic effects and their possible detection using GRACE. *Journal of Geophysical Research: Solid Earth*, 103(B12):30205–30229, December 1998. ISSN 01480227. doi: 10.1029/98JB02844. 6.2.2

John Wahr, Duncan Wingham, and Charles Bentley. A method of combining ICESat and GRACE satellite data to constrain Antarctic mass balance. *Journal of Geophysical Research: Solid Earth*, 105(B7):16279–16294, July 2000. ISSN 01480227. doi: 10.1029/2000JB900113. 2.1.3, 2.2.1

Hansheng Wang, Lulu Jia, Holger Steffen, Patrick Wu, Liming Jiang, Houtse Hsu, Longwei Xiang, Zhiyong Wang, and Bo Hu. Increased water storage in North America and Scandinavia from GRACE gravity data. *Nature Geoscience*, 6(1):38–42, January 2013. ISSN 1752-0894, 1752-0908. doi: 10.1038/ngeo1652. 2.1.3

Pippa L. Whitehouse, Michael J. Bentley, Glenn A. Milne, Matt A. King, and Ian D. Thomas. A new glacial isostatic adjustment model for Antarctica: Calibrated and tested using observations of relative sea-level change and present-day uplift rates. *Geophysical Journal International*, 190(3):1464–1482, September 2012. ISSN 0956-540X. doi: 10.1111/j.1365-246X.2012.05557.x. 5.1

B. Wouters, A. Martin-Español, V. Helm, T. Flament, J. M. van Wessem, S. R. M. Ligtenberg, M. R. van den Broeke, and J. L. Bamber. Dynamic thinning of glaciers on the Southern Antarctic Peninsula. *Science*, 348(6237):899–903, May 2015. ISSN 0036-8075, 1095-9203. doi: 10.1126/science.aaa5727. 2.2.2

H. Jay Zwally, Jun Li, Anita C. Brenner, Matthew Beckley, Helen G. Cornejo, John DiMarzio, Mario B. Giovinetto, Thomas A. Neumann, John Robbins, Jack L. Saba, Donghui Yi, and Weili Wang. Greenland ice sheet mass balance: Distribution

of increased mass loss with climate warming; 2003–07 versus 1992–2002. *Journal of Glaciology*, 57(201):88–102, 2011. ISSN 0022-1430, 1727-5652. doi: 10.3189/002214311795306682. 2.1.1

庭野匡思, 青木輝夫, 橋本明弘, 大島長, 瑞王梶野, 大沼友貴彦, 藤田耕史, 山口悟, 島田利元, 竹内望, 津滝俊, 本山秀明, 石井正好, 杉山慎, 平沢尚彦, and 阿部彩子. 氷床表面質量収支の実態とそのモデリングの試み： 2020年夏最新版. 雪氷, 83(1):27–50, 2021. doi: 10.5331/seppyo.83.1_27. 5.2